Original Article

MOLECULAR METABOLISM

GPS2-mediated regulation of the adipocyte secretome modulates adipose tissue remodeling at the onset of diet-induced obesity

Justin English [1,2], Joseph Orofino [1], Carly T. Cederquist [1], Indranil Paul [1,5], Hao Li [6], Johan Auwerx [6], Andrew Emili [1,5], Anna Belkina [3,4], Dafne Cardamone [1], Valentina Perissi [1,7,*]

ABSTRACT

Objective: Dysfunctional, unhealthy expansion of white adipose tissue due to excess dietary intake is a process at the root of obesity and Type 2 Diabetes development. The objective of this study is to contribute to a better understanding of the underlying mechanism(s) regulating the early stages of adipose tissue expansion and adaptation to dietary stress due to an acute, high-fat diet (HFD) challenge, with a focus on the communication between adipocytes and other stromal cells.

Methods: We profiled the early response to high-fat diet exposure in wildtype and adipocyte-specific GPS2-KO (GPS2-AKO) mice at the cellular, tissue and organismal level. A multi-pronged approach was employed to disentangle the complex cellular interactions dictating tissue remodeling, via single-cell RNA sequencing and FACS profiling of the stromal fraction, and semi-quantitative proteomics of the adipocyte-derived exosomal cargo after 5 weeks of HFD feeding.

Results: Our results indicate that loss of GPS2 in mature adipocytes leads to impaired adaptation to the metabolic stress imposed by HFD feeding. GPS2-AKO mice are significantly more inflamed, insulin resistant, and obese, compared to the WT counterparts. At the cellular level, lack of GPS2 in adipocytes impacts upon other stromal populations, with both the eWAT and scWAT depots exhibiting changes in the immune and non-immune compartments that contribute to an increase in inflammatory and anti-adipogenic cell types. Our studies also revealed that adipocyte to stromal cell communication is facilitated by exosomes, and that transcriptional rewiring of the exosomal cargo is crucial for tissue remodeling. Loss of GPS2 results in increased expression of secreted factors promoting a TGFβ-driven fibrotic microenvironment favoring unhealthy tissue remodeling and expansion.

Conclusions: Adipocytes serve as an intercellular signaling hub, communicating with the stromal compartment via paracrine signaling. Our study highlights the importance of proper regulation of the 'secretome' released by energetically stressed adipocytes at the onset of obesity. Altered transcriptional regulation of factors secreted via adipocyte-derived exosomes (AdExos), in the absence of GPS2, contributes to the establishment of an anti-adipogenic, pro-fibrotic adipose tissue environment, and to hastened progression towards a metabolically dysfunctional phenotype.

Keywords Adipose tissue; Obesity; Cellular communication; scRNA-seq; Exosome; GPS2

1. INTRODUCTION

The white adipose tissue (WAT) is a highly expansile endocrine organ, capable of matching the metabolic conditions of which it is presented. A critical aspect of the adaptation to conditions of excess food intake is tissue expansion to meet the increased demand for energy storage. Tissue expansion occurs through either an increase in the size of existing adipocytes (hypertrophy) or an increase in adipocyte number through de novo differentiation (hyperplasia) [61,100,144,150,160], with the modality of expansion being critical in determining metabolic fitness of the obese state [150,159]. For a complete understanding of the mechanisms behind tissue expansion, it is critical to consider the complex cellular composition of the adipose tissue, which includes not only mature adipocytes, but also adipose stem and progenitor cells (ASPC), vascular cells, and a variety of immune cells, collectively known as the stromal vascular fraction (SVF) [9,30,50,88,89,125]. The

[1]Department of Biochemistry, Boston University School of Medicine, Boston, MA, USA [2]Department of Pharmacology and Experimental Therapeutics, Boston University School of Medicine, Boston, MA, USA [3]Flow Cytometry Core Facility, Boston University School of Medicine, Boston, MA, USA [4]Department of Pathology and Laboratory Medicine, Boston University School of Medicine, Boston, MA, USA [5]Center for Network Systems Biology, Boston University, Boston, MA, USA [6]Laboratory of Integrative Systems Physiology, Interfaculty Institute of Bioengineering, Ecole Polytechnique Federale de Lausanne, Lausanne, Switzerland [7]School of Life Science, Northwestern Polytechnical University, Xi'an 710072, China

*Corresponding author. Department of Biochemistry, Boston University School of Medicine, Boston, MA, USA

E-mails: Jtenglis@bu.edu (J. English), Jorofino@bu.edu (J. Orofino), Ctcederq@gmail.com (C.T. Cederquist), Indranil@bu.edu (I. Paul), Hao.li@nwpu.edu.cn (H. Li), Johan.auwex@epfl.ch (J. Auwerx), Aemili@bu.edu (A. Emili), Abelkina@bu.edu (A. Belkina), Dafneina@gmail.com (D. Cardamone), vperissi@bu.edu (V. Perissi).

Received December 26, 2022 • Accepted January 22, 2023 • Available online 31 January 2023

https://doi.org/10.1016/j.molmet.2023.101682

recent advent of single-cell RNA sequencing technologies has allowed for the teasing apart of SVF heterogeneity, thus providing a framework for understanding the plasticity of WAT under differing conditions of nutrient intake [15,39,42,68,74,111,132,139,158]. Changes in abundance and function of stromal cell populations, as well as communication between fat-storing adipocytes and other cell types, have emerged as critical-albeit incompletely understood-components of the adaptive response to obesogenic stimuli.

G-Protein Pathway Suppressor 2 (GPS2) is a small, ubiquitously expressed protein originally identified as a suppressor of Ras activation in yeast [146], and a component of the NCoR/SMRT transcriptional corepressor complex in mammalian cells [174]. Work done by us and others revealed that GPS2 plays a central role in the regulation of cellular homeostasis through modulation of cholesterol and triglyceride metabolism, regulation of mitochondrial biogenesis, and inhibition of inflammation [18,19,41,51,64,75,136,153,157]. These processes are modulated by GPS2 through a combination of genomic and non-genomic functions, that rely, at least in part, on the inhibition of non-degradative ubiquitination by the E2 conjugating enzyme Ubc13 [92].

Here, we have utilized a mouse model of adipocyte-specific GPS2-knockout (GPS2-AKO) to study the adaptive response to acute metabolic stress imposed by a 5 week, 60% high-fat diet (HFD) through a combination of single-cell RNA sequencing, FACs analysis, and semi-quantitative proteomics. Previous work indicates that adipo-specific deletion of GPS2 leads to increased body weight gain and adiposity, due to a combination of defective thermogenesis, reduced mitochondrial content and increased insulin signaling across different depots [18,21,41], however striking differences in the metabolic fitness of obese GPS2-null mice were reported. Intriguingly, obesity was found to be uncoupled from inflammation and metabolic dysfunction in chow-fed mice GPS2-AKO mice [21], whereas GPS2-AKO mice exposed to HFD presented increased inflammation and more severe insulin resistance than their leaner, wild type littermates [40,41]. Based on these phenotypic discrepancies observed under different dietary conditions, we profiled GPS2-AKO mice response to short-term HFD with the goal of investigating the molecular mechanisms underpinning the early stages of development of insulin resistance and inflammation, independently of those contributing to obesity, and to investigate the impact of adipocyte adaptation, or lack of thereof, on adipose tissue remodeling and expansion.

2. METHODS

2.1. Bioinformatic analyses using omics data from mouse cohorts

Phenome-wide association studies (PheWAS) results for Gps2 was retrieved from https://www.systems-genetics.org/phewas [93]. Phenotype and Gps2 expression data from the CTB6F2 cohort (F2 cross cohort between CAST/EiJ and C57BL/6J) [138] was downloaded from GeneNetwork (http://genenetwork.org/).

2.2. Animal studies & metabolic analysis

Previously generated fat-specific GPS2 knockout mice (GPS2-AKO) were utilized along with wildtype littermate controls. All experiments used male mice between 6 and 8 weeks of age. For details of generation of the mouse line, please see [21]. Mice were maintained on a 60% high-fat diet (HFD) (Research Diets, D12492i) for 5 weeks. Insulin tolerance tests (ITT) were performed at the completion of HFD feeding. Mice were starved for 4 h, and blood glucose levels were measured first at time zero, and then at 15-minute intervals up to 1 h, following an initial IP injection of insulin (Humulin R, Lilly) (0.5 U/kg body weight). Blood is obtained through tail vein nicking and measured using a OneTouch Ultra glucometer. All animal studies were approved by the Boston University Institutional Animal Care and Use Committee (IACUC) and performed in strict accordance with NIH guidelines for animal care.

2.3. H&E staining

Following mouse euthanasia, subcutaneous and epididymal adipose tissue was incubated at 4 deg C in 10% neutral buffered formalin solution (Sigma) overnight. Tissues were then transferred to 70% ethanol, paraffin embedded, sectioned, stained with hematoxylin & eosin following the standard protocols employed by the Tufts Medical School Animal Histology Core.

2.4. Immunofluorescence staining, imaging, & quantification

Tissue sections were first deparaffinized and washed, followed by heat-mediated antigen retrieval (10 mM sodium citrate, 0.05% Tween 20, pH 6.0). From there, slides were then permeabilized for 45 min at room temperature in buffer (0.2% Triton X-100 in PBS) and a hydrophobic barrier was drawn around each tissue section using the A-PAP pen (Sigma). Slides were then washed in blocking solution (10% donkey serum, 1% BSA, PBS) for 1 h at room temperature. Excess blocking buffer was removed, and primary antibody was added to each section (1:100 dilution in blocking solution; Galectin 3 monoclonal antibody, eBioscience, ThermoFisher Scientific). After three washes of 5 min each with PBS, slides were incubated with secondary antibody for 1 h at room temperature, light protected (Cy5-conjugated AffiniPure Donkey Anti-Rat IgG, Jackson ImmunoResearch Laboratories). Slides were then washed three times for 5 min each with PBS, and ProLong Gold antifade reagent with DAPI mounting medium (Invitrogen by ThermoFisher Scientific) was applied (2 drops per slide), followed by a coverslip. Slides were dried for 1 h at room temperature in the dark, and then edges of each coverslip were sealed with nail polish. For longer-term storage and prior to imaging, slides were kept at 4 deg C in the dark. Stained slides were imaged on a Zeiss Axio Observer fluorescence microscope at 20× magnification. Images were analyzed and processed for publication using FIJI.

2.5. Protein isolation and western blot analysis

Protein extracts were prepared from mouse primary adipocytes or whole tissue through homogenization in lysis buffer (50 mM HEPES, pH 7.4, 40 mM NaCl, 2 mM EDTA, 1.5 mM $NaVO_4$, 50 mM NaF, 10 mM sodium pyrophosphate, 10 mM sodium β-glycerophosphate, 1% Triton X-100, 0.1% SDS, 1% sodium deoxycholate). Lysates were centrifuged for 5 min, 1000 rpm in order to remove triglyceride layer. Concentrations were analyzed using the Bradford assay (Biorad) and normalized for protein loading. The following antibodies were used for western blotting: Rb Phospho-AKT ser473 (193H12) (#4058T, 1:1000, Cell Signaling), Rb Total AKT (#9272S, 1:1000, Cell Signaling).

2.6. Isolation of primary adipocytes and stromal vascular cells from mouse adipose tissue

Upon completion of 5 week 60% high-fat diet (HFD), C57BL6/J WT and GPS2-AKO mice were euthanized, and adipose tissue depots (subcutaneous and epididymal, scWAT and eWAT respectively) were excised. The tissue was then minced in cold PBS in a tissue culture dish, and filtered through 250 micron mesh. Following filtration, the minced tissue was placed in a 50 mL Falcon tube with collagenase type 1 (Worthington Biochemical Corporation) digestion buffer (eWAT: 0.025 g collagenase, 0.5 g BSA; scWAT: 0.05 g collagenase, 0.5 g BSA). The total buffer volume is 25 mL DMEM media (with 4.5 g/L glucose & L-glutamine, without sodium pyruvate). The Falcon tubes were then placed in a shaker for at least 1 h at 37°, moving at 120

RPM. Depending on the initial size of the depot, the time in the shaker can be increased in order to facilitate more adequate digestion. Following digestion, the milieu was filtered through 250 micron mesh and transferred to a new Falcon tube. In order to neutralize digestion, 5 mL FBS was added. The layer of lipid-laden adipocytes floating to the top of the suspension was removed, and the remaining volume was spun down at 500×*g* for 10 min to pellet the cells that constitute the stromal vascular fraction (SVF).

2.7. Single-cell RNA sequencing sample preparation & bioinformatic analysis

Following SVF preparation from digested adipose tissue, the cells were resuspended in 200 uL 1X PBS (calcium and magnesium free) containing 0.04% BSA. The cells were then quantified using a hemocytometer, and 10×3'v3 RNA libraries were generated and quantified on a bioanalyzer for mean size, concentration, and molarity within the smear range, displayed via electropherogram results. We then proceeded to Illumina Sequencing on the NextSeq 500 within the Microarray & Sequencing Resource Core Facility at Boston University School of Medicine. FASTQ files were generated via demultiplexing the Illumina base call files (BCL) through implementation of the Cellranger pipeline commands. Each FASTQ file was then aligned to the MM10 reference transcriptome, which was provided by 10X Genomics through the Cellranger count command. An aggregate of samples was then created via the Cellranger Aggr command in order to create a single matrix for downstream analysis using a Scanpy and Seurat combination. Cell QC was performed by plotting the distribution for counts per barcode, number of genes per barcode, and percent of reads aligned to mitochondrial genes. These distributions were applied in order to filter out outliers by visual thresholding. Gene counts were then normalized to 10,000 reads per cell using a counts per million normalization. The data was then logarithmized using the log1 Scanpy transformation function. Genes with a high degree of variability were selected by their mean to variance ratios using the Scanpy highly variably genes function. Each gene was scaled to unit variance following effects of total counts per cell and percent mitochondrial genes expressed being regressed out of the data. Visualization of the data was done through neighborhood graphs using the PCA representation of the matrix, and this was generated using the Scanpy Neighbors function and was embedded in 2D using the UMAP projection. Neighborhood graph clustering was performed using the Leiden Graph Clustering Methhod, and marker genes for each cluster's identity were determined by a Wilcoxon rank sum test. This test compared the expression of genes in a single cluster vs all of the other clusters combined. Differential expression analysis was performed within clusters between WT and KO samples, and was performed through application of the MAST (Model-based Analysis of Single-cell Transcriptomics) statistical framework, developed and offered on github by the Gottardo Lab at the Fred Hutchinson Cancer Research Center (Seattle, WA).

2.8. mRNAseq analysis

mRNAseq libraries were subjected to basic quality control and read trimming using the FASTQC and Trimmomatic packages. Trimmomatic was run in paired end mode with the following parameters:LEADING: 3 TRAILING: 3 SLIDINGWINDOW:4:15 MINLEN:50. Trimmed reads were analyzed using Salmon with default parameters to obtain mRNA abundance estimates using the Gencode M10 reference containing protein-coding and lncRNA transcripts. Principal component analysis was performed to visually inspect samples for the presence of potential outliers. One wild-type sample from the epididymal isolated adipocytes was dropped from the analysis. Abundance estimates were concatenated into a single matrix and filtered by removing genes with an average mean of <10. Normalization and differential expression of the abundance matrix was performed using DESeq2 with a design formula including factors for litter and condition. Differentially expressed genes were considered significant with a FDR <0.1.

2.9. FACS analysis

Purification of SVF cells was done as described above. Analyses were performed using 34 anti-mouse antibodies, split between immune and non-immune panels. For the immune, the following antibodies were used: BUV395 anti-CD11b (BD Biosciences), BUV661 anti-CD4 (BD Biosciences), BUV737 anti-CD80 (BD Biosciences), BUV805 anti-CD8 (BD Biosciences), BV421 anti-CD206 (Biolegend), e450 anti-CD19 (Thermo Fisher), BV480 anti-F4/80 (BD Biosciences), BV510 anti-CD3 (Biolegend), BV570 anti-NK11 (Biolegend), Super Bright 645 anti-Siglec F (Thermo Fisher), BV711 anti-BST2 (Biolegend), Super Bright 780 anti-CD40 (Thermo Fisher), FITC anti-MHC2 (Biolegend), Alex Fluor 532 anti-CD45 (Thermo Fisher), PerCP-e710 anti-Mertk (Thermo Fisher), PE anti-CD103 (Biolegend), PE-Dazzle594 anti-CCR7 (Biolegend), PE-Cy5 anti-CD86 (Thermo Fisher), PE-Cy7 anti-CD64 (Biolegend), APC anti-CD370 (Biolegend), Alex Fluor 700 anti-Ly6G (BD Biosciences), APC-Fire 750 anti-CD11c (Biolegend). For the non-immune, the following antibodies were used: BUV737 anti-CD24 (BD Biosciences), Super Bright 436 anti-PDGFRα (Thermo Fisher), Super Bright 600 anti-Sca1 (Thermo Fisher), PE-Cy7 anti-CD38 (Biolegend), Spark Blue 550 anti-CD45 (Biolegend), PerCP-e710 anti-CD29 (Thermo Fisher), PE anti-PDGFRβ (Biolegend), PE-Dazzle594 anti-CD31 (Biolegend), FITC anti-CD34 (Miltenyi), APC anti-CD9 (Thermo Fisher), APC-Fire750 anti-Ly6C (Biolegend). Red blood cells within the SVF were first lysed briefly using 3 mL RBC lysis buffer (Biolegend). The mix was then washed using 10—12 mL FACs buffer (PBS + 2 mM EDTA + 0.5% BSA) and centrifuged at 500×*g* for 10 min. The SVF pellet was then resuspended in PBS and single cell suspensions were stained with Zombie NIR dye (Biolegend), washed with FACs buffer, pre-blocked with mouse FcBlock (Biolegend), and stained with antibody cocktails also containing Brilliant Violet buffer (BD Biosciences) along with Monocyte blocker (Biolegend) for 30 min on ice, covered. Samples were then washed with 120 uL FACs buffer and centrifuged at 500×*g* for 10 min, twice, and then resuspended with a final volume of 120 uL FACs buffer. Ultracomp eBeads Plus (Thermo Fisher) stained with each of the previously mentioned antibodies were used for compensation. All data were acquired on the Cytek Aurora flow cytometer (Cytek). At least 100,000 events were collected per sample, with analysis performed using FlowJo 10.8. Results presented are from four independent experiments, and statistical significance is established through calculation of two-tailed Welch's *t* test. Interrogation of specific statistical measures include frequency of parent, which is the percentage of cells in the gated population out of the parent population one level up, as well as median fluorescence intensity, which is the number of molecules of a particular marker present on a specific population gated cells.

2.10. Adipocyte-derived Exosome isolation, quantification, and functional application

Exosomes were isolated from primary adipocyte conditioned media utilizing the Exo-spin™ mini Exosome Purification Kit (Cell Guidance Systems, Protocol Version 8.0). Ad-Exo suspensions were injected using a syringe pump on the Nanosight NS300 instrument (Malvern Panalytical), coupled with a sCMOS camera. Analysis was performed using the Nanosight NTA (nanoparticle tracking analysis) software,

version 3.4 (Malvern Panalytical). For all assays, exosomes were utilized within a range of 10^9—10^{11} particles/mL.

2.11. Exosome protein extraction

EV pellets were solubilized in GuHCl lysis buffer [6 M GuHCl, 100 mM Tris pH 8.5, 10 mM tris(2-car- boxyethyl)phosphine, 40 mM 2-chloroacetamide] and heated for 5 min at 95 °C. Lysates were cooled on ice for 10 min, sonicated (Branson probe sonifier 10% duty cycle, 3 times, 20 s), and heated again (95 °C for 5 min). Lysates were centrifuged for 30 min at 10,000g at 4 °C, and cleared supernatant was removed to a clean tube. GuHCl concentration was diluted to less than 0.75 M using 100 mM Tris pH 8.5, and the samples were incubated overnight at 37 °C with trypsin (1:50 w/w). The reaction was stopped by adding trifluoroacetic acid to a final concentration of 0.1%, and the peptides were desalted using C18 Sep-Pak cartridges.

2.12. Secretome analysis by mass spectrometry

Peptides were analyzed with easy-nLC 1100 (Proxeon) coupled to Q-Exactive HF-X. Raw MS files were analyzed by MaxQuant 1.6 with the Andromeda search engine. Tandem MS spectra were searched against the "Reference proteome" of mouse (taxonomic ID 10090) downloaded from UniProt. The search included variable modifications of methionine oxidation and N-terminal acetylation and fixed modification of cysteine carbamidomethylation. Peptides of minimum 7 amino acids and maximum 2 missed cleavages were allowed for the analysis. False discovery rate of 1% was used for the identification of peptides and proteins. As per standard practice, all 'contaminants' and 'reverse hits' were removed and the data sets were log transformed and quantile normalized before evaluating for statistically significant changes.

2.13. *In vitro* adipocyte differentiation

To differentiate primary mouse adipocytes, the stromal vascular fraction (SVF) was isolated from subcutaneous and epididymal adipose tissue after collagenase digestion as described above. The SVF was resuspended in DMEM with 4.5 g/L glucose & L-glutamine, without sodium pyruvate, and with 10% bovine calf serum (BCS) (HyClone) and 1% pen/strep. Once the cells reached two days past confluence, adipogenic differentiation was induced using a cocktail comprised of insulin, IBMX, and DEX, along with 10% fetal bovine serum (FBS) replacing the BCS in the media. After two days, the induction media is removed and replaced with maintenance media (DMEM with 4.5 g/L glucose & L-glutamine, without sodium pyruvate, and with 10% FBS and 1% pen/strep for 10 days).

2.14. Oil-Red O staining

Staining was performed on primary *in vitro* differentiated adipocytes fixed in 10% neutral buffered formalin at room temperature for 30 min. Fixed cells were then incubated in working solution (3:2 ratio stock solution to water) for 10 min at room temperature (Oil Red O Stock solution made with 0.5 g of oil Red powder dissolved in 100 mL of isopropanol and then sterile filtered using a syringe and a 0.20 uM filter (Corning Incorporated)). Cells were then washed with water several times to remove excess stain and any precipitate that forms prior to imaging.

2.15. RNA isolation, cDNA synthesis, & RT-qPCR analysis

RNA was isolated from mouse adipocytes, using a combination of phenol-chloroform extraction and the manufacturer protocol for the RNeasy Kit (QIAGEN). Synthesis of cDNA was performed using the Biorad iScript cDNA Synthesis System, followed by SYBR-green qPCR amplification. Data normalization was performed using amplification of housekeeping gene *CyclophilinA*, and all qPCRs were performed in triplicate for each biological replicate. Data are expressed as sample mean between triplicate experiments +/− SEM. Statistical significance for all experiments was calculated by Welch's *t* test.

2.16. Omics data availability

Genomics Data were deposited to SRA with submission ID SUB11770965, BioProject ID PRJNA858249. Proteomics Data were deposited on Proteome Xchange with submission ID 1-20220712-511.

3. RESULTS

3.1. Genetic association between obesity-related traits and GPS2 expression and gene variants

To investigate GPS2 relevance in protecting against obesity and metabolic disorders, we first took advantage of the BXD inbred mouse cohort, the largest and most extensively characterized murine genetic reference panel for investigating gene-by-environment interaction [2,4,94]. Unbiased reverse genetic phenome-wide association studies (PheWAS) revealed a strong genetic association between obesity-related traits and GPS2 gene variants (Figure 1A). Significant correlations between numerous obesity-related traits and GPS2 expression levels in adipose tissue were also recorded in the F2 cross cohort between CAST/EiJ and C57BL/6J (CTB6F2), for both male and female mice [138] (Figure 1B). These results are in accord with GPS2 deletion leading to cellular hypertrophy and accumulation of triglycerides in human adipocytes [6] and with the increased adiposity observed in adipose-specific GPS2-null mouse models [21,40,41]. Previous genetic association studies in humans had also revealed a significant correlation between the down-regulation of GPS2 at the onset of obesity and the development of obesity-associated inflammation [153]. This is in accord with the observation that HFD-fed, GPS2-AKO mice are not only more obese than their WT counterparts, but also more inflamed and insulin-resistant [40,41,51]. However, it is noteworthy that the obesity developed by GPS2-AKO mice under chow diet remains uncoupled from insulin resistance and inflammation, at least in part due to enhanced insulin signaling [21]. These results, together, indicate that GPS2 plays a critical role in the maintenance of adipose tissue homeostasis, and suggested that a better characterization of these contrasting phenotypes provided a unique opportunity for investigating the mechanism(s) regulating adipose tissue expansion and cellular adaptation to dietary stress.

3.2. Characterization of adipocyte-specific GPS2-AKO mice exposed to short term HFD

To best characterize the underlying mechanisms that contribute to failed adaptation to dietary stress in GPS2-AKO mice, we first sought to determine the point at which GPS2-null mice begin exhibiting metabolic dysfunction when switched from chow to HFD feeding. To this end, we tracked weekly the body weight gain of male mice between 6 and 8 weeks of age under a 60% HFD. In accord with the pattern previously observed under chow diet [21], weights between littermate mice begin to diverge within the first 2—3 weeks, with the AKO mice weighing significantly more than the WT by week 4—5 (Figure 1C). Based on this kinetic, we examined the ability of the mice to clear glucose through insulin tolerance testing after 5 weeks of HFD. As seen in Figure 1D, by 5 weeks GPS2-AKO mice are significantly more insulin resistant than their WT counterparts, as evidenced by the delayed insulin-induced glucose clearance over time. These results are in accord with long term studies in which early signs of insulin resistance and low-grade meta-inflammation in GPS2 KO were observed after 4 weeks of HFD feeding [40,41,51].

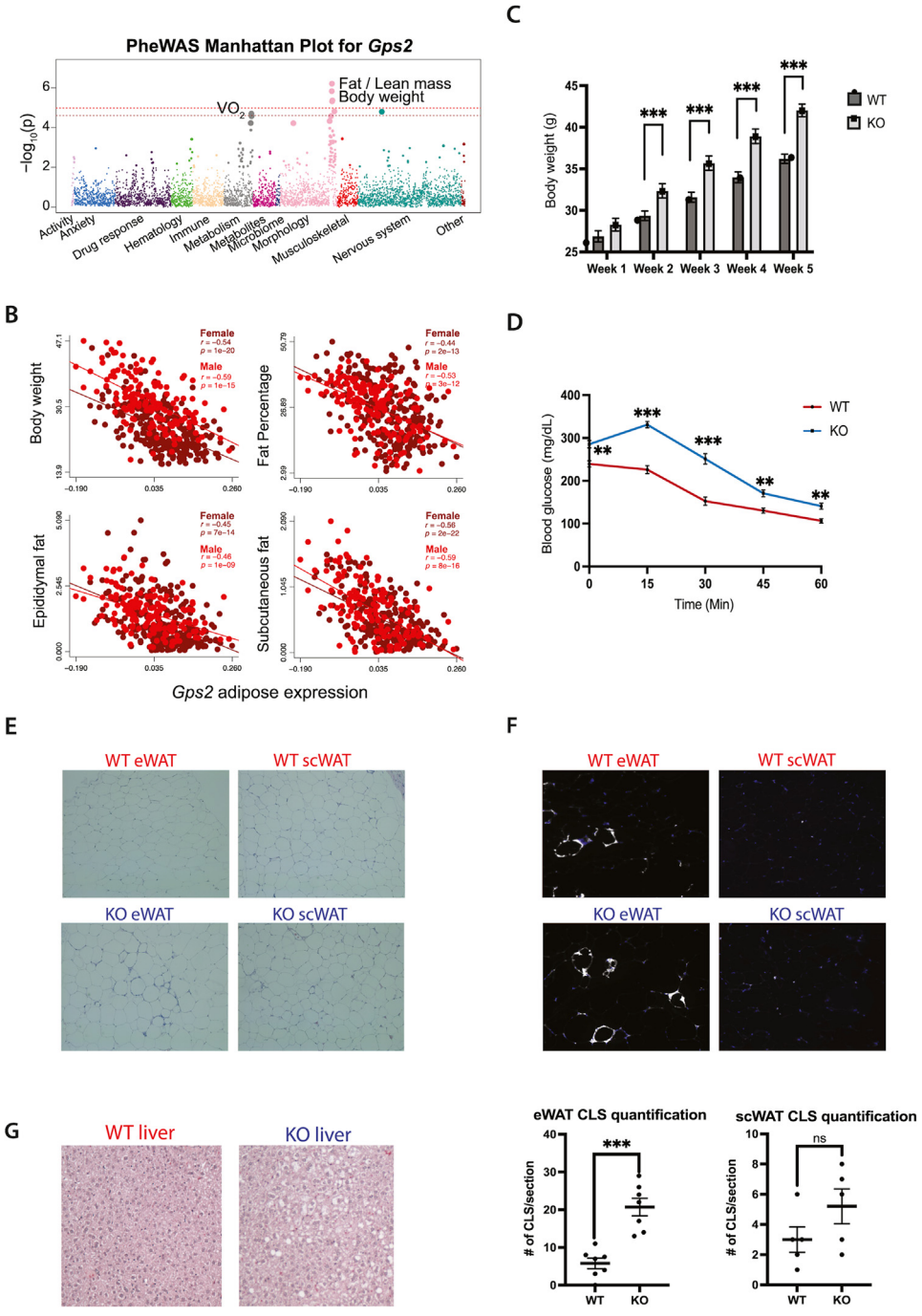

Figure 1: GPS2 function is critical in maintaining metabolic health at the cellular, tissue, and whole organism level. (A) Manhattan plot for GPS2 shows genetic association between obesity related traits and GPS2 gene variants in the BXDs. Phenotypes were arranged and colored according to respective phenotypic categories. Phenome-wide significance was determined based on Bonferroni correction using the total number (upper red dashed line) as well as the effective number (lower dark red dashed line) of phenotypes. Significant phenotypes include: *-log$_{10}$(p) 6.21, Fat mass after activity wheel_HFD, males (g)*; *-log$_{10}$(p) 5.83, Body weight after activity wheel_HFD, males (g)*; *-log$_{10}$(p) 5.36, Lean mass as percentage of body weight after activity wheel_HFD, males (%)*; *-log$_{10}$(p) 5.32, Fat mass as percentage of body weight after activity wheel_HFD, males (%).* (B) Pearson correlations between obesity and adipose tissue related traits and expression levels of GPS2 in the adipose tissue of CTB6F2 mice; red dots indicate males, dark red dots indicate females. (C) Significant body weight gain in GPS2-AKO mice compared to WT littermates with weekly monitoring, n = 22 WT, 20 KO. (D) Insulin tolerance test (ITT) following completion of 5 week, 60% high-fat diet regimen; mice were injected i.p. with 0.5U/kg body weight insulin following a 4 h fasting period, n = 15 WT, 16 KO. (E) Representative H&E staining of paraffin embedded epididymal and subcutaneous white adipose tissue sections imaged at 10× magnification. (F) Crown-like structure quantification as performed via immunofluorescence staining performed on eWAT and scWAT sections imaged at 20× magnification, using the Mac2/Galectin 3 monoclonal antibody; both representative images and quantification are shown, n = 7 WT, 7 KO for eWAT and n = 5 WT, 5 KO for scWAT. (G)Representative H&E staining of paraffin embedded liver sections imaged at 10× magnification. All quantification results are presented as mean ± SEM. Statistical significance for all experiments was calculated by Welch's *t* test; **signifies p value ≤ 0.01, ***signifies p value ≤ 0.001.

Next, we performed phenotypic profiling of adipose tissue and other metabolic organs at this early stage to investigate the appearance of inflammatory marks and ectopic lipid deposition in GPS2-AKO mice as compared to matching WT littermates. While profiling of neither epididymal (eWAT) or subcutaneous (scWAT) adipose tissue depots by H&E staining showed significant adipocyte hypertrophy (Figure 1E), eWAT sections from GPS2-AKO mice displayed a dramatic increase in the appearance of crown-like structure (CLS), a histological hallmark indicative of macrophages surrounding dead or dying adipocytes (Figure 1E). This represent a major phenotypic difference with chow-fed GPS2-AKO mice in which we did not observe any sign of inflammation in presence of similar or higher body weight [21]. As a means of confirming and quantifying these findings, we performed immunofluorescence staining for macrophages with the Galectin 3/Mac-2 antibody. As depicted in Figure 1F, a significantly higher number of CLS was observed in the eWAT of AKO mice as compared to WT littermates, whereas no differences were recorded in the scWAT. At this stage, neither eWAT nor scWAT presented evidence of fibrosis by Picro-sirius red staining regardless of the genotype (Supplemental Fig. S1A). Also, no major differences were observed in skeletal muscle gross morphology (Supplemental Fig. S1B). In contrast, representative liver sections from GPS2-AKO mice showed budding lipid droplets at the time when none is yet observed in WT livers (Figure 1G). Thus, together, these results indicate that the switch from the metabolically healthy phenotype observed under a chow diet to the more inflamed and dysfunctional phenotype reported after long term HFD occurs within the first few weeks of HFD feeding, at the time when the adipose tissue of GPS2-AKO mice has not yet reached the expansion capacity that in older chow-fed mice remained associated with insulin sensitivity [21]. Notably, at this stage, AKT signaling is still enhanced in adipose tissue from GPS2-AKO mice as compared to WT littermates (Supplemental Fig. S1C), in accord with previous reports of insulin resistance setting in prior to the disruption of AKT signaling [63,116,170].

3.3. Single-cell RNA sequencing of WAT SVF following short-term HFD reveals GPS2-dependent changes in stromal composition

To further characterize GPS2-regulated, diet-induced changes in the cellular composition of the adipose tissue, we compared collagenase-isolated SVF from eWAT and scWAT of WT and GPS2-AKO littermates after 5 weeks of 60% HFD by scRNA-seq (2 male mice/genotype, 2000 cells/mouse, depth 35K reads, 2K genes/cell). Clustering analysis of all reads combined, following current best practices [54,155,164,179], identified a number of immune and non-immune populations comparable to those described by others, including macrophages, dendritic cells, NK, B and T cells, in addition to several distinct adipose precursor subpopulations (named eAP1-3 in the eWAT and scAP1-5 in the scWAT) [15,42,47,68,115,132,139] (Figure 2A,B, Supplemental Figs. S2A and S2B, Supplemental Tables 1 and 2). Adipose precursors included both *Pdgfrα*—expressing multipotent progenitor populations (eAP1-2, scAP1-2 and scAP4-5) (Figure 2C) and more committed preadipocytes (eAP3 and scAP3) characterized by the expression of adipogenic markers such as *PPARγ, Fabp4, Lpl, Fabp5, Car3, and CD36* (Figure 2D) [15,29,56,59,68-176]. Comparison of our data with the characterization of mouse white adipose tissue cell populations across eWAT and inguinal (iWAT) depots recently published by Emont and colleagues [47] shows that in the scWAT SVF, the *Pdgfrα*$^{+}$*, Dpp4*$^{+}$*, Pi16*$^{+}$ scAP1 and scAP5 early progenitor clusters strongly overlaps with mASPC2 and partially with mASPC3, whereas *Pdgfrα*$^{+}$*, Pdgfrβ*$^{+}$ scAP2 and scAP4 clusters include cells further down in the differentiation path as shown by partial overlap with mASPC1 and mASPC6 in addition to mASPC3, and by the expression of adipogenic markers such as *Lpl, Adgfr5 and FABP4* (Figure 2C and Supplemental Tables 1 and 2). Similarly, in the eWAT, comparative analysis between the top 100 DEG defining each cluster indicates that the *Pdgfrα*$^{+}$*, Dpp4*$^{+}$*, Pi16*$^{+}$ eAP2 progenitor population share 65% of marker genes with mASPC2 and almost 50% with mASPC3, whereas *Pdgfrα*$^{+}$*, Pdgfrβ*$^{+}$ eAP1 closely resembles mASPC3 with some overlap with mASPC1 and mASPC6, representing more differentiated clusters previously shown to expand upon HFD [47] and to align with differentiating ASC's from Burl et al., committed preadipocytes from Hepler et al., and the *Fabp4*+ "G2" cluster from Schwalie et al. [15,68,139]. In agreement with this characterization, scAP1, scAP5 and eAP2 also share defining genes with the Ly6c1^{+} FIPS fibro-inflammatory progenitors, and the *Ebf2*$^{+}$ G1 and FAP3 progenitors previously reported by other groups [15,137,139], while scAP2 and eAP1 appear to encompass the *Cd142*+ Areg precursors first described by Schwalie et al. and later shown to overlay with mASPC4 [47,139] (Figure 2E and Supplemental Fig. S2C, Supplemental Tables 1 and 2).

Next, we analyzed the scRNAseq data separated by genotype. As expected, we did not observe any change in GPS2 expression within the stromal compartment, thus confirming that deletion is specific to mature adipocytes (Supplemental Fig. S2D). To identify, in an unbiased manner, cell clusters that differ in abundance between WT and AKO mice we used scCODA, a Bayesian model for addressing cell-type compositional differences between conditions [16]. Using WT as covariate condition, this approach led to the identification of the eAP3 preadipocyte population as the only cluster significantly different between WT and KO mice (Supplemental Fig. S2E). Beyond the changes identified through stringent analysis by scCODA, we also observed trending changes in the proportions of other clusters that appeared consistent across the littermate replicates (Figure 2F, Supplemental Fig. S2E). In eWAT, this includes an increase in the abundance of *Pdgfrα*$^{+}$ eAP1 and eAP2 progenitors (clusters 2 and 3), and B-cells (cluster 8), a decrease in dendritic cells (cluster 5), and changes in the respective abundance of different macrophage subpopulations (cluster 0 and 1) (Figure 2F, left). In the scWAT, we observed an increase in pro-inflammatory M1 macrophages (cluster 3), and the appearance of collagen-expressing macrophages (cluster 7) and scAP4/scAP5 progenitors (cluster 10 and 14) (Figure 2F, right). Together, these results indicate that loss of GPS2 in mature adipocytes leads to broad changes in adipose tissue composition, at the level of both immune and non-immune cell types, which underlie the overall response to excess nutrients intake.

3.4. Flow cytometric profiling of stromal populations following 5-week 60% HFD highlights depot- and genotype-dependent differences in ASPCs

As a means of validating and quantifying the changes identified by the scRNAseq, we designed a comprehensive panel of cell markers that allow for measurement of immune and non-immune cell types and used it to profile by FACS the eWAT and scWAT SVF of mice exposed to 5 weeks of HFD feeding. The non-immune panel includes 11 markers selected based upon prior research on adipose stem cells and established flow cytometry panels (Supplementary Table 3) [27,68,101,104,106,121,134,178]. The immune panel contains 23 markers, also curated based upon established literature [27,68,101,104,106,121,134,178] (Supplementary Table 3). All antibodies were optimized and validated using both spleen and adipose tissue samples.

First, we characterized the non-immune compartment of the eWAT. While there was no significant difference in the overall abundance of

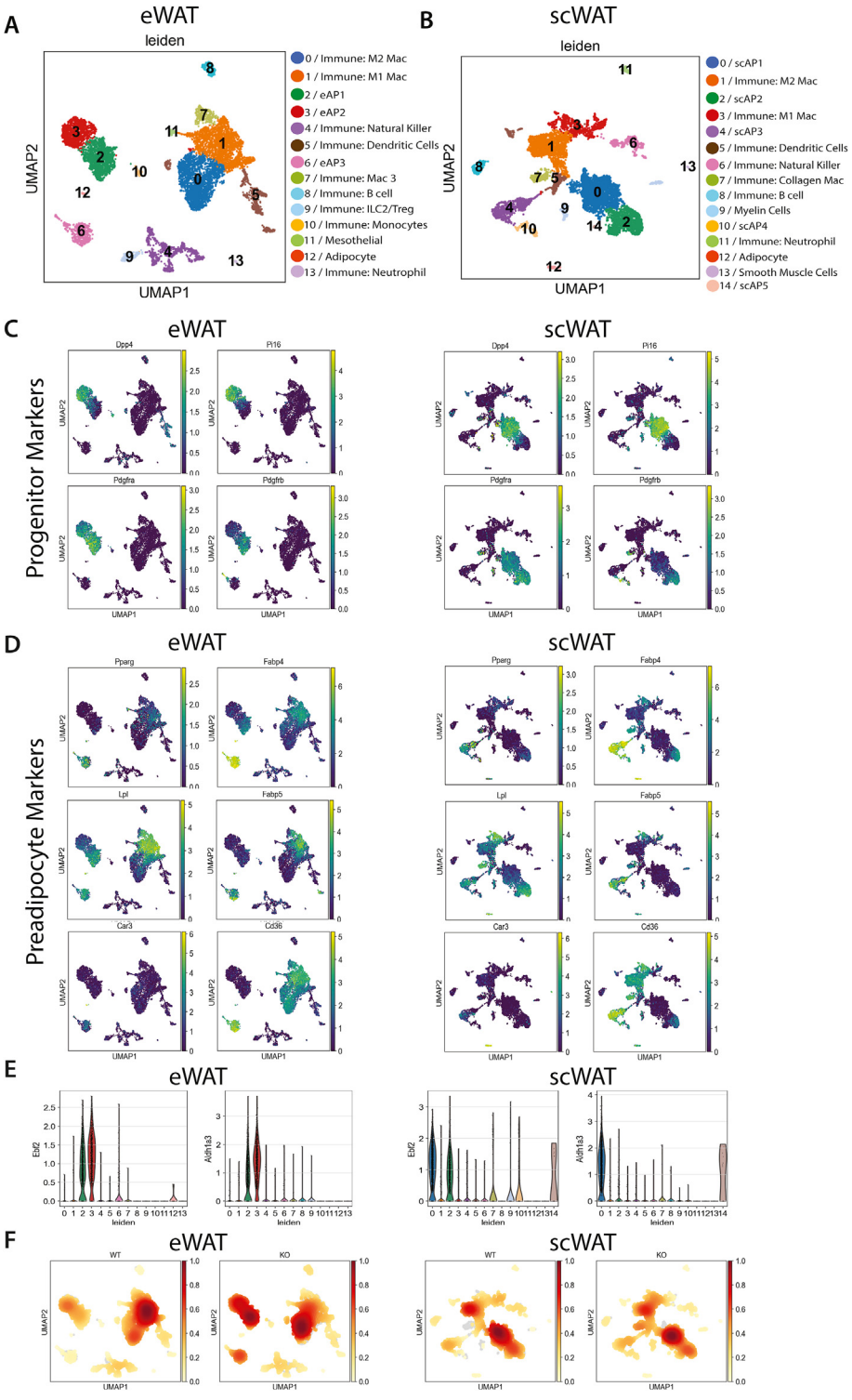

Figure 2: Single-cell RNA sequencing of SVF from eWAT and scWAT of WT and GPS2-AKO mice following 5 week, 60% HFD reveals clustering unique to each depot. (A) Leiden plot of cell clusters identified in eWAT, with associated legend outlining 14 distinct populations. (B) Leiden plot of cell clusters identified in scWAT, with associated legend outlining 15 distinct populations. (C) Heat map expression levels of markers used to define early adipocyte progenitors, overlayed with our scRNAseq clustering in both eWAT and scWAT. (D) Heat map expression levels of markers used to define committed preadipocytes, overlayed with our scRNAseq clustering in both eWAT and scWAT. (E) Violin plots outlining the expression of select early adipose progenitor markers *Ebf2* and *Aldh1a3* across all eWAT and scWAT clusters identified in our scRNAseq. (F) Changes in the proportions of eWAT and scWAT clusters as assessed by heat maps for both WT and GPS2-AKO littermate replicates.

$CD45^{-}CD31^{-}CD34^{+}$ ASPCs (Figure 3A), we observed a shift in progenitor subtypes (Figure 3B). In particular, using the same gating strategy used by Hepler and colleagues [68], we observed a significant increase in $Ly6C^{+}CD9^{+}$ fibro-inflammatory and anti-adipogenic precursors in the eWAT of AKO mice as compared to their WT littermates. On the converse, $Ly6C^{-}CD9^{+}$ MLCs (mesothelial-like cells) showed a noticeable decrease in AKO mice, albeit not a statistically significant change (Figure 3B). No significant differences were observed in the abundance of classic $Ly6C^{-}CD9^{-}$ adipogenic 'APCs' (adipocyte precursor cells) (Figure 3B). In contrast, in the scWAT we did record an increase in the overall abundance of ASPCs accompanied by a decrease in the proportion of CD45+ immune cells (Figure 3C).

Next, we interrogated if the expression of specific markers revealed any differences in the signature of these populations between WT and AKO. We compared the median fluorescence intensity (MFI) measured for established progenitor and preadipocyte markers, including SCA-1, CD34, CD24, CD38, PDGFRα and PDGFRβ [20,76,90,130]. across WT and AKO samples, as well as quantification of the markers separated by progenitor population for the eWAT. While we did not observe substantial differences between the two genotypes in neither eWAT or scWAT depots at large, in the eWAT we observed significant differences within the $CD9^{+}Ly6C^{-}$ compartment in the expression of CD38 (decreased in AKO) and PDGFRα (increased in AKO) (Supplemental Fig. 3A). Recent single cell profiling of *Wt1*$^{+}$ cells has shown that mesothelial cells do not differentiate into adipocytes [163], thus suggesting that this result may reflect an accumulation of pluripotent adipose progenitors at the expense of more committed precursors, rather than actual gene expression changes in mesothelial cells per se. Altogether, these findings confirm that adipocyte-specific deletion of GPS2 associates with the accumulation of ASPCs, including an increase in the eWAT in the abundance of fibro-inflammatory progenitors previously shown to display anti-adipogenic properties [68].

3.5. Flow cytometric profiling of the adipose immune compartment highlights genotype-dependent differences in macrophage recruitment and identity

Similar to the methodology used for the non-immune compartment, we also investigated by FACS the impact of adipo-specific GPS2 deletion on the immune compartment. Based on the differential clustering observed by RNA-seq and the increase in CLS, we focused on B cells, Dendritic cells, and Macrophage populations. As expected upon HFD [28,55,70,99,114], macrophages gated on the basis of general markers CD11b and F4/80 are strongly represented in both AT depots (Figure 3D). Macrophages were also found significantly increased in the scWAT of AKO mice as compared to WT littermates (Figure 3D,E). When dissecting the different macrophage subtypes based on presence of selective markers, we observed three distinct populations, shown via representative plots in Figure 3F, that correspond to classically activated M1 macrophages ($CD11c^{high}$,$CD206^{low}$), alternatively activated M2 macrophages ($CD11c^{low}$,$CD206^{high}$), and $CD11c^{high}$,$CD206^{high}$ M2-like macrophages [117,118]. The M2-like are more greatly represented in the eWAT than scWAT, whereas the classic M1 subtype is more abundant in the scWAT (Figure 3E,F). In comparing these populations across littermates, we found that the proportion of M2 cells was increased, most significantly in the eWAT, in the SVF of AKO mice (Figure 3E,F). As shown in Supplemental Fig. 4A, no significant differences were observed between WT and AKO when examining the expression of CD206 or CD11c, nor in the expression of these markers across the two depots, regardless of genotype. In contrast, comparing the MFI of specific markers of macrophage activation/subtypes within specific subpopulations revealed a decrease in CD86 and CD40 expression in M2 cells from eWAT AKO mice as compared to WT (Supplemental Fig. 4B) thus pointing towards possible differences in macrophage-dependent T cell activation [113]. We also recorded a near significant increase in the expression of CD64 in M2-like cells from the scWAT of AKO mice as compared to WT littermates, which could be indicative of increased polarization of this subtype towards an M1 phenotype in accord with the increase in macrophages with an M1 signature observed by scRNAseq [134] (Supplemental Fig. 4B).

Lastly, we addressed other immune cell types of interest. No differences were observed in the abundance of B cells, which comprise a small fraction compared to the rest of the cellular milieu, between WT and AKO mice, nor in the expression level of CD19, an essential B-cell marker, via MFI quantification (Supplemental Fig. 4C). There was also no significant difference between WT and AKO in terms of: (i) overall dendritic cells abundance, as defined by MHCII and CD11c expression (Supplemental Fig. 4D); (ii) proportion of conventional cDC1 and cDC2 subtypes, which was found to be skewed, as expected, towards the cDC2 phenotype (Supplemental Fig. 4D) [7,26,69,103,145,147]; (iii) the expression of specific DC markers via MFI quantification (Supplemental Fig. 4E) [13,31,71,161,175].

Overall, these results indicate that the major impact of GPS2 deletion in adipocytes, in term of both cell number and functional profile of immune cells within the adipose tissue, is on the macrophage compartment, with an increase and possibly functional rewiring of $CD206^{+}$ M2 and M2-like macrophages.

3.6. Profiling of adipocyte gene expression and protein cargo of adipo-secreted EVs from WT and GPS2-AKO mice

Together, the scRNAseq and FACs results indicate that loss of GPS2 in mature adipocytes has a profound impact on the cellular composition of the adipose tissue and its reorganization upon dietary challenge, thus suggesting that GPS2 contributes to regulating the crosstalk between adipocytes and other cell types in the early phases of adaptation to HFD feeding. This led us to question how cell-to-cell communication is facilitated. Because adipocytes are endocrine cells, responsible for secreting factors that signal both locally and long-range to other organs [3,12,65,128,133,139,149], we hypothesized that loss of GPS2-mediated remodeling of gene expression in stressed adipocytes impacts upon adipose tissue expansion via altered expression of secreted factors. In accord with this hypothesis, gene expression profiling by RNAseq of adipocytes from the eWAT and scWAT WT and AKO mice exposed to 16 weeks of HFD showed an enrichment for genes involved in cell communication and inflammatory processes (visualized with EnrichR) [22,84,165] (Supplemental Table 4 and Figure 4A,B). In particular, when focusing on putative secreted factors (as defined by application of the functional annotation tool DAVID) [72,140], and visualized using ToppGene Suite [23], among DEGs from both eWAT and scWAT, we observed a significant enrichment for terms related to the extracellular matrix (ECM), including both components of the ECM as well as remodeling enzymes (Figure 4C). Genes upregulated in GPS2 null adipocytes included several collagens (COL3A1, COL14A1, COL6A5, COL1A1, COL1A2), along with matrix metallopeptidases (MMP2, MMP12, MMP13) and their inhibitors (TIMP1, TIMP2), whereas other factors associated with ECM remodeling (ADAMTS1, ADAMTS5, HTRA1, CELA1) were found downregulated together with specific adipokines (RARRES2) and cytokines (IL7) (Supplemental Fig. 5A). A similar trend was observed among genes specifically regulated only in one depot (Supplemental Fig. 5B and C), suggesting that loss of GPS2 may have a broad impact on the expression of adipocyte secreted factors in HFD-fed mice.

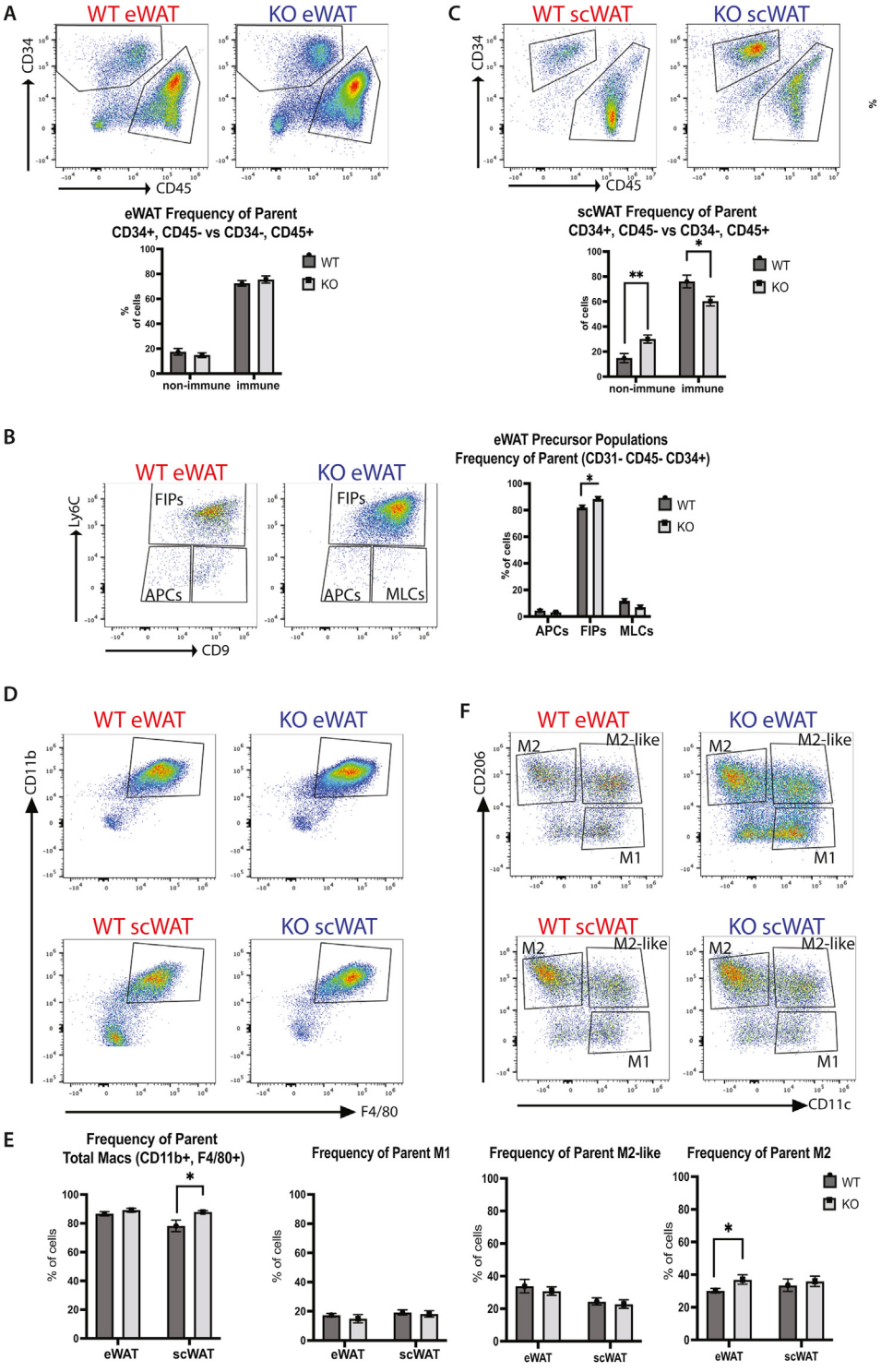

Figure 3: Comprehensive fluorescence activated cell sorting (FACS) of the SVF from WT and GPS2-AKO mice following 5 week, 60% HFD feeding, validates and quantifies changes observed in immune and non-immune cell populations first observed in scRNAseq. (A) Gating strategy implemented to separate out non-immune from immune stromal cells, on the basis of CD34 and CD45 expression, in both eWAT and scWAT. (B) Further characterization of the eWAT non-immune compartment, using a Ly6C vs CD9 gating strategy to separate out previously characterized populations known as FIPs (Ly6C+, CD9+), APCs (Ly6C-, CD9-), and MLCs (Ly6C-, CD9+). (C) Gating strategy to separate out macrophages from other immune cell subtypes, done so on the basis of general macrophage markers F4/80 and CD11b, in both eWAT and scWAT. (D) Further dissection of the macrophage compartment using markers classically associated with M1 (CD11c) and M2 (CD206) macrophage subtypes, resulting in separation of three distinct clusters: M1 (CD11c^{high}, CD206^{low}), M2 (CD11c^{low}, CD206^{high}), and M2-like (CD11c^{high}, CD206^{high}). (E) Quantification of the general macrophage and macrophage subtype gates, utilizing the frequency of parent statistic. Representative FlowJo plots and the accompanying frequency of parent statistic quantification for A,B,C,D,&E are from 4 independent biological replicates, n = 7 WT, 9 KO. All quantification results are presented as mean ± SEM. Statistical significance for all experiments was calculated by Welch's *t* test; *signifies p value ≤ 0.05, **signifies p value ≤ 0.01.

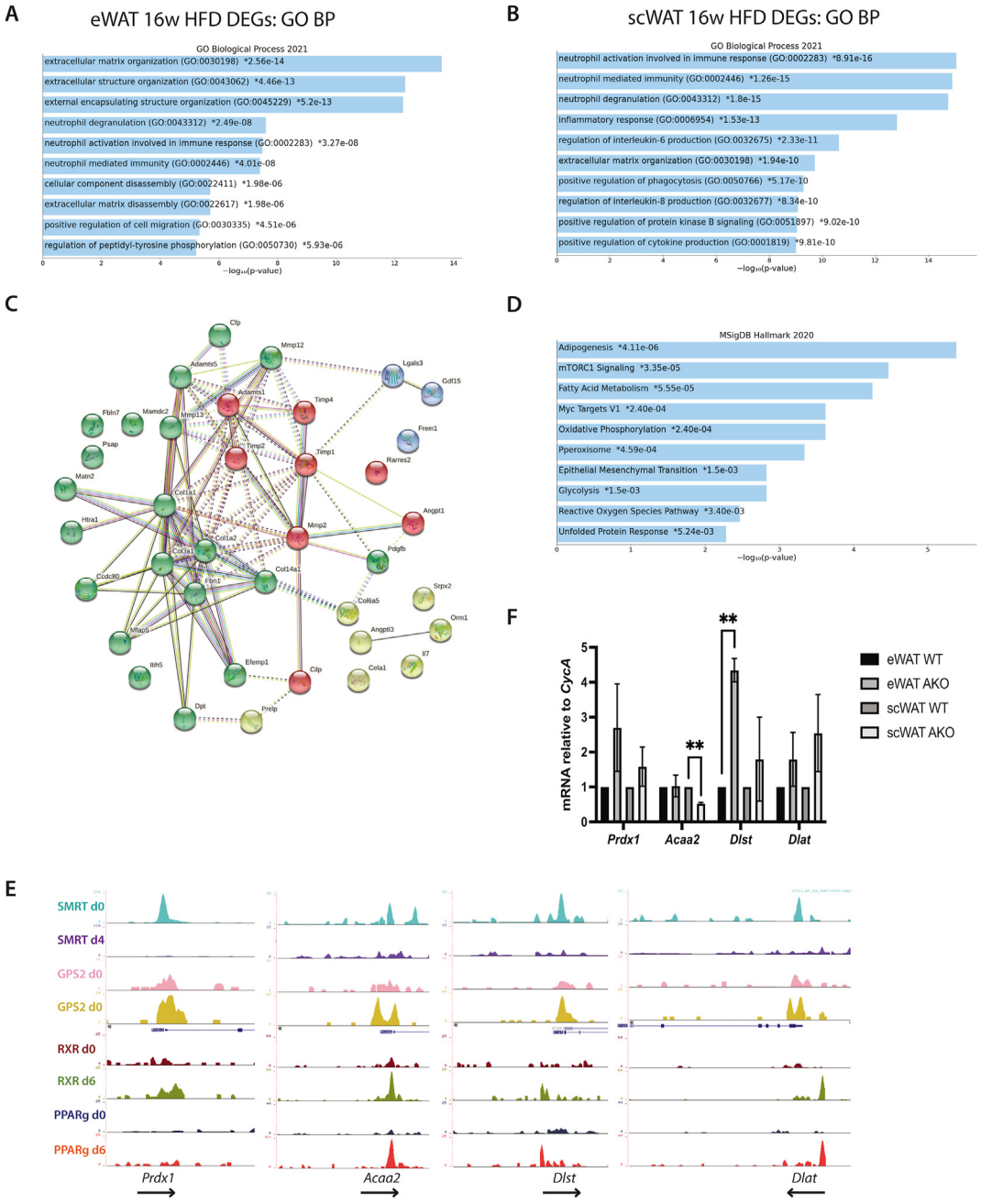

Figure 4: Adipocyte gene expression profiling from bulk RNA sequencing of adipocytes isolated from WT and GPS2-AKO mice following 16 weeks 60% HFD feeding reveals transcriptional signatures related to inflammation, cellular communication and remodeling, and metabolic reprogramming. (A) Gene ontology enrichment analysis of the upregulated differentially expressed genes from eWAT isolated adipocytes at 16 weeks of 60% HFD feeding (B) Gene ontology enrichment analysis of the upregulated differentially expressed genes from scWAT isolated adipocytes at 16 weeks of 60% HFD feeding (C) Differentially expressed factors identified in adipo-derived exosomes from the eWAT and scWAT of GPS2-AKO mice as compared to WT littermates, visualized using STRING (https:\\string-db.org) (D) Gene ontology enrichment analysis for differentially regulated secreted factors from both eWAT and scWAT AdExos. (E) ChIPseq tracks for *Prdx1, Acaa2, Dlst, and Dlat,* showing peaks for SMRT, GPS2, RXR, and PPARγ during the course of 3T3-L1 differentiation (day 0 and day 6 respectively), (F) RT-qPCR gene expression in isolated adipocytes from WT and GPS2-AKO eWAT and scWAT following 5 weeks, 60% HFD, for *Prdx1, Acaa2, Dlst, and Dlat.* Data are expressed as sample mean between triplicate experiments +/− SEM. Statistical significance for all experiments was calculated by Welch's *t* test *signifies p value $\leq$ 0.05.

In analyzing these signatures, we noticed that about half of the differentially expressed genes were previously reported as being associated with exosomes, as annotated by the Exocarta database [81,107,109,143] (Supplemental Table 4). Adipocyte-derived exosomes (AdExos) are small extracellular vesicles secreted by adipocytes and known to mediate cellular communication within the adipose tissue as well as across different organs [32,33,44,60]. To further characterize whether GPS2 deletion in adipocytes impacts the exosomal cargo, we decided to profile the protein content of exosomes released by primary adipocytes isolated from GPS2-AKO and WT mice via semi-quantitative mass spectrometry. AdExos were isolated from adipocyte-derived conditioned media following completion of the 5

week 60% HFD regimen (across two separate cohorts of mice for a total of $n = 4$ WT, *6 KO*), and subjected to protein extraction followed by LC-MS/MS analysis. Across the eWAT and scWAT, we detected 316 unique proteins, 90% of which had been previously associated with exosomal cargo, including half of the top 100 proteins that are commonly regarded as general exosome markers [81,107,109,143] and many factors previously identified as AdExo specific cargo [38,67,86] (Supplemental Table 5).

Among these candidate signaling factors, we determined those that were differentially secreted from WT and AKO adipocytes in each depot. The largest majority of differentially regulated proteins were upregulated in exosomes secreted from GPS2-AKO as compared to WT littermates (Supplementary Table 5). This included 92 proteins in AdExos from eWAT and 22 proteins from scWAT, whereas only 14 and 8 were found downregulated in eWAT and scWAT respectively. Overall the differentially regulated factors were enriched for translation factors, fatty acid metabolism (ACAA2, FASN, ECH1), glycolysis and TCA cycle (PGAM1, DLAT, GAPDH, DLST), focal adhesion and integrin signaling (THBS1, LAMB1, LAMA4, LAMC1) (Figure 4D), and thus likely involved in both remodeling of the ECM and metabolic reprogramming of target cells, as described for exosome-mediated communication across a variety of cell/tissue models [58,152,168,173].

3.7. GPS2 is required for transcriptional regulation of exosomal cargo proteins

These results confirmed that lack of GPS2 has a significant impact on the content of AdExos that are released by energy-stressed adipocytes from WT or GPS2-AKO mice at the onset of diet-induced obesity, likely due to altered gene expression of selected cargo factors. Because of the well-characterized role of GPS2 in transcriptional regulation, we next asked whether differentially regulated proteins are direct targets of GPS2 and other cofactors in the NCoR/SMRT corepressor complex. Integration of the list of proteins differentially regulated in GPS2-AKO eWAT and scWAT AdExos with previous ChIPseq datasets [17,51,153] revealed that indeed 83 out of 92 proteins upregulated in the eWAT KO and 17 out of the 22 proteins upregulated in the scWAT KO are putative targets of GPS2-mediated transcriptional regulation, based on its recruitment to the promoter region of the gene in 3T3-L1 cells and RAW macrophages (Supplemental Table 6). The large majority (65–80% depending on the depot) of these genes are also bound by SMRT and/or NCoR, indicating that GPS2 is likely recruited to their promoters as part of the NCoR/SMRT corepressor complex (Supplemental Table 6 and Figure 4E). Comparative analysis of these data sets also revealed that GPS2 binding to the promoter region remains consistent - if not increased - during 3T3-L1 differentiation, whereas NCoR and SMRT are released upon induction of adipogenesis often concomitant to PPARγ binding (Figure 4E). These observations suggest that these genes are repressed by the NCoR/SMRT corepressor complex in preadipocytes, and their expression is likely upregulated as preadipocytes differentiate into mature adipocytes. They also reveal that the contribution of GPS2 to their transcriptional regulation extends beyond basal repression, as previously shown for other PPARγ target genes [19], and suggest that the lack of GPS2 may impair the re-establishment of transcriptional repression in energy stressed adipocytes. Indeed, via RT-qPCR analysis, we observed significant or near significant upregulation of several candidate genes in GPS2-null adipocytes from either depot, as compared to WT, including *Prdx1*, *Dlst*, and *Dlat*, whereas the upregulation of others, like *Acaa2*, may depend on post-translational regulation (Figure 4F).

3.8. Impact of AdExos on adipose-to-ASPCs communication

To confirm that changes in the exosomal cargo secreted from GPS2 null adipocytes are, at least in part, responsible for the phenotypic differences in cellular composition of the SVF observed by scRNAseq and FACS in HFD-challenged mice, we assessed the effect of AdExos on adipocyte differentiation *in vitro*. Because of limited differentiation capacity of eWAT SVF *in vitro* [49,102,105,151], we used primary scWAT SVF derived from the WT and GPS2-AKO mice following the HFD regimen, and differentiated them in presence or absence of exosomes released by eWAT adipocytes isolated from either WT or AKO HFD-fed mice. As shown in Figure 5A, at baseline, addition of adipogenic cocktail results in SVF differentiation (as indicated by Oil Red O staining, a dye used for staining neutral triglycerides and lipids that is commonly used as a measure of adipocyte maturation) for both WT and GPS2-AKO-derived cells, even though the adipogenic capacity of the GPS2-AKO SVF appears to be slightly lower. Upon addition of WT AdExos to either WT or GPS2-AKO SVF, the same pattern displayed at baseline is observed. However, in presence of GPS2-KO AdExos, cell differentiation is drastically reduced, with the KO SVF in particular showing only few lipid-laden cells (Figure 5A). These results confirm that factors present in the cargo of AdExos released by GPS2-null adipocytes have a negative impact on the differentiation capacity of stromal APSCs.

To identify, among differentially expressed AdExos cargo proteins, possible mediators of direct adipocyte-to-SVF signaling, we compared the list of differentially expressed proteins with genes identified as putative receptor–ligand pairs across adipose tissue cell types via scRNAseq combined to CellPhoneDB analysis [43,47]. Out of the 92 proteins significantly upregulated in GPS2-AKO epiWAT AdExos, we found 14 "ligands" that are putative mediators of communication between adipocytes and other immune and non-immune cell types in the adipose tissue, including critical growth factors IGF2 and TGFβ1 and several collagen types. Similarly, out of 22 proteins upregulated in GPS2-AKO scWAT exos, 5 overlapped with reported ligand–receptor pairs (Supplemental Table 7). When focusing on putative mediators of adipocyte-to-ASPC communication, we identify THBS1 and LAMC1 as upregulated in both depots, as well as two collagen family members COL5A1 and COL6A2 (Figure 5B). Gene expression analysis by RT-qPCR confirmed that they are all, except for COL6A2, upregulated in GPS2 null adipocytes (Figure 5C), with their regulation likely occurring at the transcriptional level as indicated by promoter occupancy by GPS2 in differentiating adipocytes (Figure 5D). Intriguingly, these proteins are important for remodeling of the extracellular matrix towards a more fibrotic phenotype and have been associated with feed-forward loops with anti-adipogenic TGFβ signaling [1,34,52,62,83,85,91,98,112,156]. Because TGFβ itself had been identified among the proteins upregulated in GPS2-AKO eWAT AdExos (Supplemental Table 5), we measured the expression of the *Tgfb1* gene as well by RT-qPCR and found it significantly upregulated in primary adipocytes isolated from the eWAT of GPS2-AKO mice as compared to their WT counterparts (Figure 5E). Notably, interrogation of ChIPseq data confirmed that the *Tgfb1* gene is also a direct target of GPS2 transcriptional regulation (Figure 5E).

These results together suggested increased pro-fibrotic, TGFβ signaling being released through exosomes by the energy stressed adipocytes lacking GPS2, as compared to the adipocytes of WT littermates. In accord with this conclusion, inhibiting TGFβ signaling with TGFBR1 kinase inhibitor SB431542 rescues adipogenesis in presence of KO-derived AdExos (Figure 5F). Moreover, treatment with SB431542 alone provides a slight improvement in the differentiation capacity of the SVF isolated from GPS2-AKO mice (Figure 5F), suggesting that aberrant

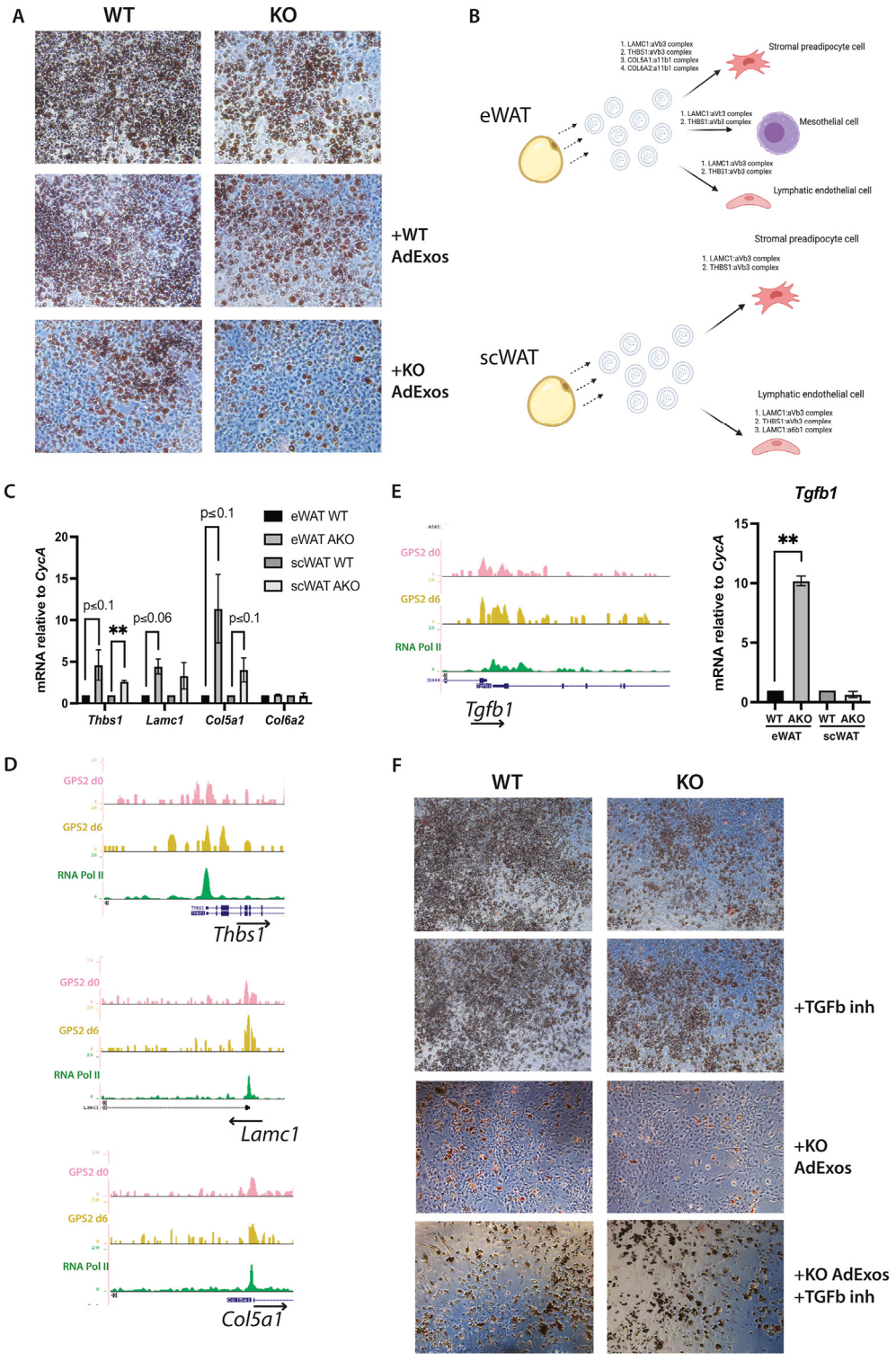

Figure 5: GPS2KO derived Ad-Exos display a functional impact on the differentiation capacity of stromal progenitor cells through exacerbation of a pro-fibrotic remodeling signature and putative direct delivery of cellular cargo. (A) Comparison of the differentiation capacity of primary WT and GPS2-AKO scWAT SVF cells following 5 week, 60% HFD, with addition of adipogenic cocktail and differing combinations of WT and GPS2-AKO AdExos. Lipid droplet accumulation is visualized by Oil Red O staining. AdExos were added within a range of 10^9-10^{11}/μL. (B) Graphical representation of CellPhoneDB analysis, highlighting shared mediators between eWAT and scWAT that represents direct adipocyte-to-SVF signaling. **Created with BioRender.com**. (C) RT-qPCR gene expression in isolated adipocytes from WT and GPS2-AKO eWAT and scWAT following 5 weeks, 60% HFD, for *Thbs1, Lamc1, Col5a1, and Col6a2*; Data are expressed as sample mean between triplicate experiments +/− SEM. Statistical significance for all experiments was calculated by Welch's *t* test, **signifies p value $\leq$ 0.01. (D) Representative ChIPseq tracks showing promoter occupancy by GPS2 in differentiating adipocytes for *Thbs1, Lamc1,* and *Col5a1*. (E) ChIPseq tracks showing promoter occupancy by GPS2 in differentiating adipocytes for *Tgfb1*, along with RT-qPCR analysis in isolated adipocytes from WT and GPS2-AKO eWAT and scWAT following 5 weeks, 60% HFD for *Tgfb1*. Data are expressed as sample mean between triplicate experiments +/− SEM. Statistical significance for all experiments was calculated by Welch's *t* test, **signifies p value $\leq$ 0.01 (F) Comparison of the differentiation capacity of primary WT and GPS2-AKO scWAT SVF cells following 5 week, 60% HFDin presence of GPS2-AKO AdExos alone or with TGFBR1 kinase inhibitor SB431542 (SB) (5 μmol/L). Lipid droplet accumulation is visualized by Oil Red O staining.

TGFβ signaling is a contributing factor to the development and maintenance of antiadipogenic progenitors in culture.

To further investigate the extent to which upregulation of TGFβ signaling may be impacting on the fate of adipose progenitors, we also analyzed the differential gene expression signature of each AP cluster previously defined by scRNAseq using the MAST statistical framework and the Seurat R toolkit [54,66], and then employed EnrichR as a means of visualizing these signatures [22,84,165] (Supplemental Table 8). Strikingly, terms related to TGFβ regulation and pro-fibrotic ECM remodeling were found significantly enriched across all eAP clusters, including ASPCs eAP1 and eAP2, and committed eAP3 (Supplemental Fig. 6A), thus confirming that changes in signaling molecules secreted from GPS2-null adipocytes promote rewiring of ASPCs gene expression. An enrichment in genes associated with TGFβ signaling was also observed among the DEGs between GPS2-AKO and WT M2 macrophage cluster, along with several inflammation/inflammatory signaling terms (Supplemental Fig. 6B). Interestingly, results consistent with a TGFβ-related enrichment were also observed for scWAT clusters scAP1, scAP2, and scAP3 (Supplemental Fig. 6C), even though elevated expression of TGFB1 was restricted to the eWAT at both protein and mRNA level. Collectively, these results support that gene expression signatures of both immune and non-immune stromal cells at the onset of obesity are remodeled towards a pro-fibrotic and anti-adipogenic profile in response to signals driven by GPS2-null, energy stressed adipocytes

4. DISCUSSION

Diet-induced adipose tissue expansion is a complex adaptive response that requires coordinated reprogramming of many different cell types and thus relies on rewiring of intercellular communication pathways. Here, we have shown that failed rewiring of exosome-mediated signaling from energy stressed adipocytes to other stromal cells at the onset of obesity contributes to accelerated progression towards metabolic dysfunction. Profiling of the stromal compartment of GPS2-AKO mice exposed to short term HFD through scRNA-seq and FACS has revealed that loss of GPS2 in mature adipocytes has a profound effect on the overall remodeling of eWAT and scWAT tissues, with both depots exhibiting changes in the immune profile and accumulation of anti-adipogenic progenitors. Our results indicate that transcriptional regulation by GPS2 and associated cofactors plays an essential role in the reprogramming of the adipocyte secretome. In particular, in the absence of GPS2, the transcriptional regulation of several factors that are secreted by adipocytes through adipocyte-derived exosomes (AdExos) is impaired, leading to elevated levels of TGFβ and other pro-fibrotic signaling factors in the cargo of AdExos released by GPS2-null energy-stressed adipocytes, and thus to the establishment of an anti-adipogenic and fibroinflammatory environment (Figure 6).

TGFβ signaling is known to inhibit adipogenesis and adipocyte stem cell (ASC) commitment, and its downregulation is required for adipogenesis and healthy adipose tissue remodeling, particularly in visceral tissue depots [45]; M.-J. [87]; S.-N [96,123,127,167]. In agreement with other studies [11,115,117,124,135,154], our data emphasize the importance of a fine-tuned temporal regulation of TGFβ secretion and support the hypothesis that pro-fibrotic TGFβ signaling in the adipose tissue is driven by different cell types, with adipo-derived TGFβ signaling being amplified by increased recruitment of TGFβ-secreting macrophages.

Unexpectedly, our results also indicate that adipo-derived TGFβ is, at least in part, secreted through exosomes, which may be facilitating its

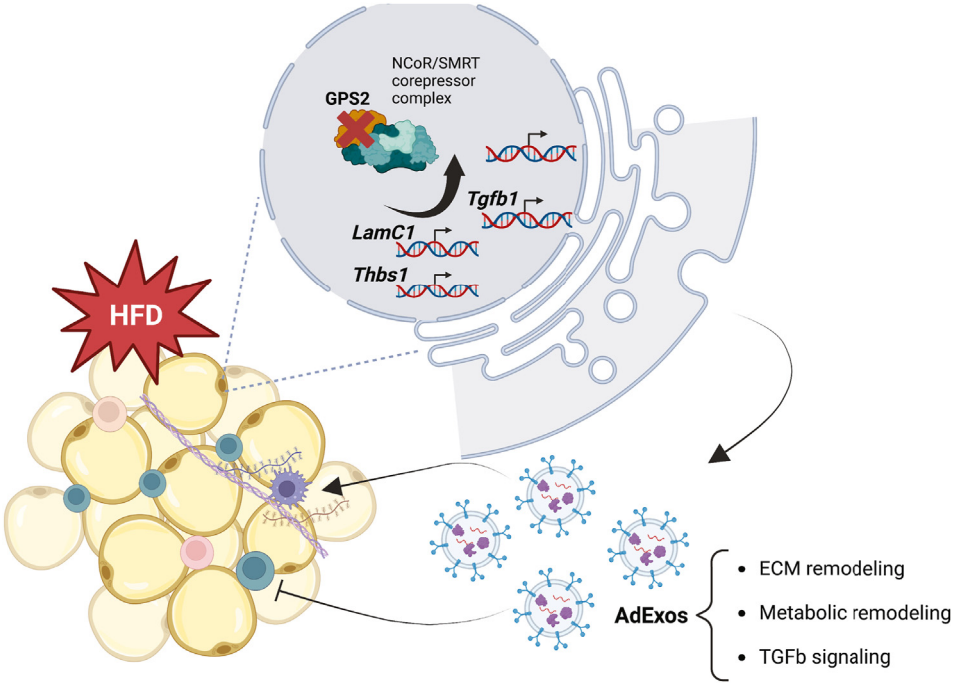

Figure 6: Impact of GPS2 deletion in adipocyte on cellular crosstalk. Schematic representation of the effects of adipose-specific GPS2 deletion on the crosstalk between energy-stressed mature adipocytes and other stromal cells. Loss of GPS2 leads to an increase in the expression of secreted factors that contribute to ECM remodeling and metabolic reprogramming of target cells. In particular, GPS2 binds to and regulates the expression of several genes that are secreted, upon translation, through Adipose-derived Exosomes (AdExos), including mediators of TGFβ signaling such as *Tgfb1, Thbs1, LamC1, Col5a1* and others. Adipo-derived signaling promotes the rewiring of gene expression in progenitor and immune target cells, contributing to the accumulation of anti-adipogenic progenitors and the rewiring of the macrophage compartment as revealed by scRNAseq.

uptake by target cells. Exosomes have recently emerged as critical players in intercellular communication [80,108,122]. Adipose-derived exosomes in particular have been associated with regulation of lipid metabolism, inflammation and insulin-resistance [166,169,171]; B [172,177,180]. However, a clear understanding of the role and relevance of exosomes secreted by different cell types within the adipose tissue and the molecular mechanisms controlling the loading of specific proteins/miRNAs into the exosomes at any given time is currently lacking. Overall, our results highlight the importance of exosomes secreted by energy-stressed adipocytes in mediating paracrine communication to other adipose stromal cells, and suggest that the gene expression profiles of both adipose macrophages and ASPC populations gets rewired towards an anti-adipogenic fate upon exposure to AdExos secreted by GPS2-null adipocytes. Integrated analysis of the mature adipocyte transcriptome and the proteome of adipocyte-derived exosomes from GPS2 WT and AKO mice exposed to short term HFD has in fact revealed that the gene expression program regulated through GPS2-mediated repression in energy stressed adipocytes, includes many anti-adipogenic exosomal proteins, including TGFβ and other pro-fibrotic factors. Intriguingly, this signature presents striking similarities with that of fibrosis-inducing exosomes secreted by tubular cells exposed to high glucose in diabetic kidney disease [162]. Based on these findings, we speculate that transcriptional rewiring of the adipo-derived exosomal cargo at the onset of diet-induced obesity is critical for promoting an environment that is conducive to healthy tissue expansion through de novo adipogenesis, as opposed to one favoring hypertrophy and tissue fibrosis.

The impact of GPS2-mediated transcriptional regulation of exosomal components on inter-organ communication processes remains to be determined, but it is important to acknowledge that exosomes contribute to long range inter-organ communication as well as to local paracrine signaling [8,25,36,57,82,126]. This suggests that the altered exosomal content observed in the absence of GPS2 may also play a direct role in contributing to the worsening of whole body metabolic fitness in addition to the indirect effects caused by increased lipid spillover, enhanced local inflammation, and cytokine and adipokine signaling. As an example, loss of adipose GPS2 was found to be inhibitory for insulin secretion from pancreatic islets [40]. As AdExos were recently involved in adipose-pancreas crosstalk [60], future studies should investigate the extent to which altered expression of their cargo may play a role in this process. In the absence of GPS2, for example, we observed the upregulation of *Dbi,* a factor with a well-established record of involvement in pancreatic signaling and regulation of body mass homeostasis and obesity [10,77,97,142]. that may be relevant to the modulation of insulin secretion by beta cells.

Other exosomal factors found upregulated in the absence of GPS2 instead are good candidates for mediating the communication between adipocytes and adipose stromal cells. Among them LAMC1, COL5A1, and THBS1 were previously identified as candidate ligands for signaling to ASPCs and macrophages [47] and are known as important ECM regulators and profibrotic signaling molecules [14,24,37,78,110]. Glycoprotein Thrombospondin-1 (THBS1), in particular, is an adipokine acutely upregulated in obesity with established connections to adipose inflammation, insulin resistance, and modulation of preadipocyte proliferation [83,98,156]. THBS1 was shown to activate fibrotic tissue damage by promoting collagen deposition and to participate in a feed forward loop in which it licenses the activation of latent TGFβ and is activated by TGFβ through SMAD3 transcription [35]. *Thbs1* expression is tightly regulated at the transcriptional level, and previous studies highlighted the importance of a negative regulatory region located in the same area where we recorded GPS2/SMRT occupancy [148]. Intriguingly, an enrichment for thrombospondin genes was also present in human adipose-derived exosomes shown to promote breast cancer progression and epithelial—mesenchymal transition (EMT), thus showing a thread worth pursuing about the role of exosomal cargo rewiring in the adaptation to obesity and its impact on the pathogenesis and progression of cancer in obese and diabetic patients [73].

Mechanistically, our results indicate that the maladaptive rewiring of the exosomal cargo in the absence of GPS2 includes the upregulation of several profibrotic genes through transcriptional derepression. Indeed, most of the factors we found differentially regulated in exosomes secreted by GPS2-null adipocytes are transcriptionally repressed by the GPS2-containing NCoR/SMRT corepressor complex in preadipocytes and are marked by both GPS2 and PPARγ promoter occupancy in differentiating adipocytes. Based on structural evidences about the interplay between different corepressors in the NCoR/SMRT corepressor complex [120], we propose that compromised assembly of the NCoR/SMRT corepressor complex in the absence of GPS2 may explain the observed increase in gene expression. This provides a mechanistic explanation for failed rewiring of the exosomal cargo secreted by energy stressed adipocytes in GPS2-AKO mice exposed to a short-term dietary challenge, in a similar fashion to the derepression of inflammatory cytokines reported in GPS2-null macrophages [153], and adds to a large body of literature highlighting the importance of NCoR/SMRT corepressors and associated cofactors in the modulation of lipid metabolism, adipose tissue functions, and metabolic health [5,46,48,53,79,95,119,129,131,141]. Future studies investigating the extent to which this can be rescued by modulating aberrant ubiquitination activity in the absence of GPS2 may provide useful translational insights for the treatment of obesity and associated metabolic disorders. The fact that common regulatory strategies are employed for modulating the expression of multiple factors converging on promoting a maladaptive phenotype, in particular, may provide unique opportunities for developing therapeutic approaches targeting the mechanism of increased secretion rather than aiming at blocking individual profibrotic factors.

DATA AVAILABILITY

Omics data are included in Supplementary table and raw data deposited on the public repositories SRA and Proteome Xchange.

ACKNOWLEDGMENTS

We are grateful to past and current members of the Perissi Lab and colleagues in the Departments of Biochemistry and Medicine for feedback and insightful discussions, with particular acknowledgments to Drs. Jude Deeney, Tova Meshulam, Nabil Rabhi, Steve Farmer and Andrew Tilston-Lunel. We also thank Drs. Gerald Denis, Naser Jafari, Manohar Kolla and Carla Mazzeo for assistance with exosome isolation and characterization. In addition, we are thankful for the assistance of Dr. Nathan Li and the Tufts Medical Center Animal Histology Core, Dr. Yuriy Alekseyev and the BUSM Single Cell Sequencing Core, and the Boston Nutrition Obesity Research Center (BNORC) Functional Genomics Core (P30DK046200). This work was supported by the following awards: NIGMS Training Grant in Biomolecular Pharmacology 5T32GM008541-22 to JE, NIDDK Training grant in Obesity, Endocrinology, and Metabolism 5T32DK007201-44 to JE and JO, NIDDK R01DK100422, P30DK046200 and NIGMS R01GM127625 to VP.

CONFLICT OF INTEREST

The authors have no competing interests to declare

APPENDIX A. SUPPLEMENTARY DATA

Supplementary data to this article can be found online at https://doi.org/10.1016/j.molmet.2023.101682.

REFERENCES

[1] Altun Ö, Arman Y, Yoldemir ŞA, Pala AS, Gümüşkaya PÖ, Özcan M, et al. The association of laminin levels with insulin resistance and non-alcoholic hepatosteatosis. Diabetol Metab Syndrome 2021;13(1):60. https://doi.org/10.1186/s13098-021-00682-z.

[2] Andreux PA, Williams EG, Koutnikova H, Houtkooper RH, Champy M-F, Henry H, et al. Systems genetics of metabolism: the use of the BXD murine reference panel for multiscalar integration of traits. Cell 2012;150(6):1287–99. https://doi.org/10.1016/j.cell.2012.08.012.

[3] Antonopoulos AS, Tousoulis D. The molecular mechanisms of obesity paradox. Cardiovasc Res 2017;113(9). https://doi.org/10.1093/cvr/cvx106.

[4] Argmann CA, Chambon P, Auwerx J. Mouse phenogenomics: the fast track to "systems metabolism. Cell Metabol 2005;2(6):349–60. https://doi.org/10.1016/j.cmet.2005.11.002.

[5] Armour SM, Remsberg JR, Damle M, Sidoli S, Ho WY, Li Z, et al. An HDAC3-PROX1 corepressor module acts on HNF4α to control hepatic triglycerides. Nat Commun 2017;8(1):549. https://doi.org/10.1038/s41467-017-00772-5.

[6] Barilla S, Liang N, Mileti E, Ballaire R, Lhomme M, Ponnaiah M, et al. Loss of G protein pathway suppressor 2 in human adipocytes triggers lipid remodeling by upregulating ATP binding cassette subfamily G member 1. Mol Metabol 2020;42:101066. https://doi.org/10.1016/j.molmet.2020.101066.

[7] Bertola A, Ciucci T, Rousseau D, Bourlier V, Duffaut C, Bonnafous S, et al. Identification of adipose tissue dendritic cells correlated with obesity-associated insulin-resistance and inducing Th17 responses in mice and patients. Diabetes 2012;61(9):2238–47. https://doi.org/10.2337/db11-1274.

[8] Bischoff JP, Schulz A, Morrison H. The role of exosomes in intercellular and inter-organ communication of the peripheral nervous system. FEBS (Fed Eur Biochem Soc) Lett 2022;596(5):655–64. https://doi.org/10.1002/1873-3468.14274.

[9] Bora P, Majumdar AS. Adipose tissue-derived stromal vascular fraction in regenerative medicine: a brief review on biology and translation. Stem Cell Res Ther 2017;8(1). https://doi.org/10.1186/s13287-017-0598-y.

[10] Borboni P, Magnaterra R, Porzio O, Fusco A, Sesti G, Bertoli A, et al. DBI mRNA is expressed in endocrine pancreas and its post-translational product DBI(33-50) inhibits insulin release. Endocrine 1995;3(4):267–71. https://doi.org/10.1007/BF03021404.

[11] Bourlier V, Sengenès C, Zakaroff-Girard A, Decaunes P, Wdziekonski B, Galitzky J, et al. TGFbeta family members are key mediators in the induction of myofibroblast phenotype of human adipose tissue progenitor cells by macrophages. PLoS One 2012;7(2):e31274. https://doi.org/10.1371/journal.pone.0031274.

[12] Bradley RL, Cleveland KA, Cheatham B. The adipocyte as a secretory organ: mechanisms of vesicle transport and secretory pathways. Recent Prog Horm Res 2001;56. https://doi.org/10.1210/rp.56.1.329.

[13] Brown CC, Gudjonson H, Pritykin Y, Deep D, Lavallée V-P, Mendoza A, et al. Transcriptional basis of mouse and human dendritic cell heterogeneity. Cell 2019;179(4):846–863.e24. https://doi.org/10.1016/j.cell.2019.09.035.

[14] Buras ED, Converso-Baran K, Davis CS, Akama T, Hikage F, Michele DE, et al. Fibro-adipogenic remodeling of the diaphragm in obesity-associated respiratory dysfunction. Diabetes 2019;68(1):45–56. https://doi.org/10.2337/db18-0209.

[15] Burl RB, Ramseyer VD, Rondini EA, Pique-Regi R, Lee Y-H, Granneman JG. Deconstructing adipogenesis induced by β3-adrenergic receptor activation with single-cell expression profiling. Cell Metabol 2018;28(2):300–309.e4. https://doi.org/10.1016/j.cmet.2018.05.025.

[16] Büttner M, Ostner J, Müller CL, Theis FJ, Schubert B. scCODA is a Bayesian model for compositional single-cell data analysis. Nat Commun 2021;12(1):6876. https://doi.org/10.1038/s41467-021-27150-6.

[17] Cardamone MD, Krones A, Tanasa B, Taylor H, Ricci L, Ohgi KA, et al. A protective strategy against hyperinflammatory responses requiring the nontranscriptional actions of GPS2. Mol Cell 2012;46(1):91–104. https://doi.org/10.1016/j.molcel.2012.01.025.

[18] Cardamone MD, Tanasa B, Cederquist CT, Huang J, Mahdaviani K, Li W, et al. Mitochondrial retrograde signaling in mammals is mediated by the transcriptional cofactor GPS2 via direct mitochondria-to-nucleus translocation. Mol Cell 2018;69(5):757–772.e7. https://doi.org/10.1016/j.molcel.2018.01.037.

[19] Cardamone MD, Tanasa B, Chan M, Cederquist CT, Andricovich J, Rosenfeld MG, et al. GPS2/KDM4A pioneering activity regulates promoter-specific recruitment of PPARγ. Cell Rep 2014;8(1):163–76. https://doi.org/10.1016/j.celrep.2014.05.041.

[20] Carrière A, Jeanson Y, Côté J-A, Dromard C, Galinier A, Menzel S, et al. Identification of the ectoenzyme CD38 as a marker of committed pre-adipocytes. Int J Obes (2005) 2017;41(10):1539–46. https://doi.org/10.1038/ijo.2017.140.

[21] Cederquist CT, Lentucci C, Martinez-Calejman C, Hayashi V, Orofino J, Guertin D, et al. Systemic insulin sensitivity is regulated by GPS2 inhibition of AKT ubiquitination and activation in adipose tissue. Mol Metabol 2017;6(1). https://doi.org/10.1016/j.molmet.2016.10.007.

[22] Chen EY, Tan CM, Kou Y, Duan Q, Wang Z, Meirelles GV, et al. Enrichr: interactive and collaborative HTML5 gene list enrichment analysis tool. BMC Bioinf 2013;14:128. https://doi.org/10.1186/1471-2105-14-128.

[23] Chen J, Bardes EE, Aronow BJ, Jegga AG. ToppGene Suite for gene list enrichment analysis and candidate gene prioritization. Nucleic Acids Res 2009;37:W305–11. https://doi.org/10.1093/nar/gkp427. Web Server issue).

[24] Chen P, Yu B, Li Z, Chen Y, Sun Y, Wang DW. COL5A1 variants cause aortic dissection by activating TGF-β-signaling pathway. J Am Heart Assoc 2021;10(11):e019276. https://doi.org/10.1161/JAHA.120.019276.

[25] Chen S, Tang Y, Liu Y, Zhang P, Lv L, Zhang X, et al. Exosomes derived from miR-375-overexpressing human adipose mesenchymal stem cells promote bone regeneration. Cell Prolif 2019;52(5):e12669. https://doi.org/10.1111/cpr.12669.

[26] Chen Y, Tian J, Tian X, Tang X, Rui K, Tong J, et al. Adipose tissue dendritic cells enhances inflammation by prompting the generation of Th17 cells. PLoS One 2014;9(3):e92450. https://doi.org/10.1371/journal.pone.0092450.

[27] Cho KW, Morris DL, Lumeng CN. Flow cytometry analyses of adipose tissue macrophages. Methods Enzymol 2014a;537:297–314. https://doi.org/10.1016/B978-0-12-411619-1.00016-1.

[28] Cho KW, Morris DL, Lumeng CN. Flow cytometry analyses of adipose tissue macrophages. Methods Enzymol 2014b;537:297–314. https://doi.org/10.1016/B978-0-12-411619-1.00016-1.

[29] Christiaens V, van Hul M, Lijnen HR, Scroyen I. CD36 promotes adipocyte differentiation and adipogenesis. Biochim Biophys Acta 2012;1820(7):949–56. https://doi.org/10.1016/j.bbagen.2012.04.001.

[30] Cinti S. The adipose organ: morphological perspectives of adipose tissues. Proc Nutr Soc 2001;60(3). https://doi.org/10.1079/pns200192.

[31] Cochain C, Vafadarnejad E, Arampatzi P, Pelisek J, Winkels H, Ley K, et al. Single-cell RNA-seq reveals the transcriptional landscape and heterogeneity

of aortic macrophages in murine atherosclerosis. Circ Res 2018;122(12):1661–74. https://doi.org/10.1161/CIRCRESAHA.117.312509.

[32] Connolly KD, Rees DA, James PE. Role of adipocyte-derived extracellular vesicles in vascular inflammation. Free Radical Biol Med 2021;172:58–64. https://doi.org/10.1016/j.freeradbiomed.2021.04.031.

[33] Crewe C, Scherer PE. Intercellular and interorgan crosstalk through adipocyte extracellular vesicles. Rev Endocr Metab Disord 2022;23(1):61–9. https://doi.org/10.1007/s11154-020-09625-x.

[34] Dankel SN, Grytten E, Bjune J-I, Nielsen HJ, Dietrich A, Blüher M, et al. COL6A3 expression in adipose tissue cells is associated with levels of the homeobox transcription factor PRRX1. Sci Rep 2020;10(1):20164. https://doi.org/10.1038/s41598-020-77406-2.

[35] Daubon T, Léon C, Clarke K, Andrique L, Salabert L, Darbo E, et al. Deciphering the complex role of thrombospondin-1 in glioblastoma development. Nat Commun 2019;10(1):1146. https://doi.org/10.1038/s41467-019-08480-y.

[36] Deng S, Zhou X, Ge Z, Song Y, Wang H, Liu X, et al. Exosomes from adipose-derived mesenchymal stem cells ameliorate cardiac damage after myocardial infarction by activating S1P/SK1/S1PR1 signaling and promoting macrophage M2 polarization. Int J Biochem Cell Biol 2019;114:105564. https://doi.org/10.1016/j.biocel.2019.105564.

[37] Désert R, Mebarki S, Desille M, Sicard M, Lavergne E, Renaud S, et al. "Fibrous nests" in human hepatocellular carcinoma express a Wnt-induced gene signature associated with poor clinical outcome. Int J Biochem Cell Biol 2016;81(Pt A):195–207. https://doi.org/10.1016/j.biocel.2016.08.017.

[38] Deshmukh AS, Peijs L, Beaudry JL, Jespersen NZ, Nielsen CH, Ma T, et al. Proteomics-based comparative mapping of the secretomes of human Brown and white adipocytes reveals EPDR1 as a novel batokine. Cell Metabol 2019;30(5):963–975.e7. https://doi.org/10.1016/j.cmet.2019.10.001.

[39] Deutsch A, Feng D, Pessin JE, Shinoda K. The impact of single-cell genomics on adipose tissue research. Int J Mol Sci 2020;21(13). https://doi.org/10.3390/ijms21134773.

[40] Drareni K, Ballaire R, Alzaid F, Goncalves A, Chollet C, Barilla S, et al. Adipocyte reprogramming by the transcriptional coregulator GPS2 impacts beta cell insulin secretion. Cell Rep 2020;32(11). https://doi.org/10.1016/j.celrep.2020.108141.

[41] Drareni K, Ballaire R, Barilla S, Mathew MJ, Toubal A, Fan R, et al. GPS2 deficiency triggers maladaptive white adipose tissue expansion in obesity via HIF1A activation. Cell Rep 2018;24(11):2957–2971.e6. https://doi.org/10.1016/j.celrep.2018.08.032.

[42] Duerre DJ, Galmozzi A. Deconstructing adipose tissue heterogeneity one cell at a time. Front Endocrinol 2022;13:847291. https://doi.org/10.3389/fendo.2022.847291.

[43] Efremova M, Vento-Tormo M, Teichmann SA, Vento-Tormo R. CellPhoneDB: inferring cell-cell communication from combined expression of multi-subunit ligand-receptor complexes. Nat Protoc 2020;15(4):1484–506. https://doi.org/10.1038/s41596-020-0292-x.

[44] Eguchi A, Lazic M, Armando AM, Phillips SA, Katebian R, Maraka S, et al. Circulating adipocyte-derived extracellular vesicles are novel markers of metabolic stress. J Mol Med (Berl) 2016;94(11):1241–53. https://doi.org/10.1007/s00109-016-1446-8.

[45] Elsafadi M, Manikandan M, Atteya M, Abu Dawud R, Almalki S, Ali Kaimkhani Z, et al. SERPINB2 is a novel TGFβ-responsive lineage fate determinant of human bone marrow stromal cells. Sci Rep 2017;7(1):10797. https://doi.org/10.1038/s41598-017-10983-x.

[46] Emmett MJ, Lim H-W, Jager J, Richter HJ, Adlanmerini M, Peed LC, et al. Histone deacetylase 3 prepares brown adipose tissue for acute thermogenic challenge. Nature 2017;546(7659):544–8. https://doi.org/10.1038/nature22819.

[47] Emont MP, Jacobs C, Essene AL, Pant D, Tenen D, Colleluori G, et al. A single-cell atlas of human and mouse white adipose tissue. Nature 2022;603(7903):926–33. https://doi.org/10.1038/s41586-022-04518-2.

[48] Emont MP, Mantis S, Kahn JH, Landeche M, Han X, Sargis RM, et al. Silencing mediator of retinoid and thyroid hormone receptors (SMRT) regulates glucocorticoid action in adipocytes. Mol Cell Endocrinol 2015;407:52–6. https://doi.org/10.1016/j.mce.2015.03.002.

[49] Emont MP, Yu H, Jun H, Hong X, Maganti N, Stegemann JP, et al. Using a 3D culture system to differentiate visceral adipocytes in vitro. Endocrinology 2015;156(12):4761–8. https://doi.org/10.1210/en.2015-1567.

[50] Eto H, Suga H, Matsumoto D, Inoue K, Aoi N, Kato H, et al. Characterization of structure and cellular components of aspirated and excised adipose tissue. Plast Reconstr Surg 2009;124(4). https://doi.org/10.1097/PRS.0b013e3181b5a3f1.

[51] Fan R, Toubal A, Goñi S, Drareni K, Huang Z, Alzaid F, et al. Loss of the co-repressor GPS2 sensitizes macrophage activation upon metabolic stress induced by obesity and type 2 diabetes. Nat Med 2016;22(7). https://doi.org/10.1038/nm.4114.

[52] Fang L, Che Y, Zhang C, Huang J, Lei Y, Lu Z, et al. LAMC1 upregulation via TGFβ induces inflammatory cancer-associated fibroblasts in esophageal squamous cell carcinoma via NF-κB-CXCL1-STAT3. Mol Oncol 2021;15(11):3125–46. https://doi.org/10.1002/1878-0261.13053.

[53] Ferrari A, Longo R, Fiorino E, Silva R, Mitro N, Cermenati G, et al. HDAC3 is a molecular brake of the metabolic switch supporting white adipose tissue browning. Nat Commun 2017;8(1):93. https://doi.org/10.1038/s41467-017-00182-7.

[54] Finak G, McDavid A, Yajima M, Deng J, Gersuk V, Shalek AK, et al. MAST: a flexible statistical framework for assessing transcriptional changes and characterizing heterogeneity in single-cell RNA sequencing data. Genome Biol 2015;16:278. https://doi.org/10.1186/s13059-015-0844-5.

[55] Fujisaka S, Usui I, Bukhari A, Ikutani M, Oya T, Kanatani Y, et al. Regulatory mechanisms for adipose tissue M1 and M2 macrophages in diet-induced obese mice. Diabetes 2009;58(11):2574–82. https://doi.org/10.2337/db08-1475.

[56] Furuhashi M, Saitoh S, Shimamoto K, Miura T. Fatty acid-binding protein 4 (FABP4): pathophysiological insights and potent clinical biomarker of metabolic and cardiovascular diseases. Clin Med Insights Cardiol 2014;8(Suppl 3):23–33. https://doi.org/10.4137/CMC.S17067.

[57] Gabisonia K, Khan M, Recchia FA. Extracellular vesicle-mediated bidirectional communication between heart and other organs. Am J Physiol Heart Circ Physiol 2022;322(5):H769–84. https://doi.org/10.1152/ajpheart.00659.2021.

[58] Gangoda L, Boukouris S, Liem M, Kalra H, Mathivanan S. Extracellular vesicles including exosomes are mediators of signal transduction: are they protective or pathogenic? Proteomics 2015;15(2–3):260–71. https://doi.org/10.1002/pmic.201400234.

[59] Gao H, Volat F, Sandhow L, Galitzky J, Nguyen T, Esteve D, et al. CD36 is a marker of human adipocyte progenitors with pronounced adipogenic and triglyceride accumulation potential. Stem Cells (Dayton) 2017;35(7):1799–814. https://doi.org/10.1002/stem.2635.

[60] Gesmundo I, Pardini B, Gargantini E, Gamba G, Birolo G, Fanciulli A, et al. Adipocyte-derived extracellular vesicles regulate survival and function of pancreatic β cells. JCI Insight 2021;6(5). https://doi.org/10.1172/jci.insight.141962.

[61] Ghaben AL, Scherer PE. Adipogenesis and metabolic health. Nat Rev Mol Cell Biol 2019;20(4). https://doi.org/10.1038/s41580-018-0093-z.

[62] Goddi A, Schroedl L, Brey EM, Cohen RN. Laminins in metabolic tissues. Metabolism 2021;120:154775. https://doi.org/10.1016/j.metabol.2021.154775.

[63] Guilherme A, Pedersen DJ, Henchey E, Henriques FS, Danai Lv, Shen Y, et al. Adipocyte lipid synthesis coupled to neuronal control of thermogenic programming. Mol Metabol 2017;6(8):781–96. https://doi.org/10.1016/j.molmet.2017.05.012.

[64] Guo C, Li Y, Gow C-H, Wong M, Zha J, Yan C, et al. The optimal corepressor function of nuclear receptor corepressor (NCoR) for peroxisome proliferator-activated receptor γ requires G protein pathway suppressor 2. J Biol Chem 2015;290(6). https://doi.org/10.1074/jbc.M114.598797.

[65] Halberg N, Wernstedt-Asterholm I, Scherer PE. The adipocyte as an endocrine cell. Endocrinol Metab Clin N Am 2008;37(3). https://doi.org/10.1016/j.ecl.2008.07.002.

[66] Hao Y, Hao S, Andersen-Nissen E, Mauck WM, Zheng S, Butler A, et al. Integrated analysis of multimodal single-cell data. Cell 2021;184(13):3573–3587.e29. https://doi.org/10.1016/j.cell.2021.04.048.

[67] Hartwig S, de Filippo E, Göddeke S, Knebel B, Kotzka J, Al-Hasani H, et al. Exosomal proteins constitute an essential part of the human adipose tissue secretome. Biochim Biophys Acta, Proteins Proteomics 2019;1867(12):140172. https://doi.org/10.1016/j.bbapap.2018.11.009.

[68] Hepler C, Shan B, Zhang Q, Henry GH, Shao M, Vishvanath L, et al. Identification of functionally distinct fibro-inflammatory and adipogenic stromal subpopulations in visceral adipose tissue of adult mice. Elife 2018;7. https://doi.org/10.7554/eLife.39636.

[69] Hildreth AD, Ma F, Wong YY, Sun R, Pellegrini M, O'Sullivan TE. Single-cell sequencing of human white adipose tissue identifies new cell states in health and obesity. Nat Immunol 2021;22(5):639–53. https://doi.org/10.1038/s41590-021-00922-4.

[70] Hill DA, Lim H-W, Kim YH, Ho WY, Foong YH, Nelson VL, et al. Distinct macrophage populations direct inflammatory versus physiological changes in adipose tissue. Proc Natl Acad Sci USA 2018;115(22). https://doi.org/10.1073/pnas.1802611115.

[71] Hongo D, Zheng P, Dutt S, Pawar RD, Meyer E, Engleman EG, et al. Identification of two subsets of murine DC1 dendritic cells that differ by surface phenotype, gene expression, and function. Front Immunol 2021;12. https://doi.org/10.3389/fimmu.2021.746469.

[72] Huang DW, Sherman BT, Lempicki RA. Systematic and integrative analysis of large gene lists using DAVID bioinformatics resources. Nat Protoc 2009;4(1):44–57. https://doi.org/10.1038/nprot.2008.211.

[73] Jafari N, Kolla M, Meshulam T, Shafran JS, Qiu Y, Casey AN, et al. Adipocyte-derived exosomes may promote breast cancer progression in type 2 diabetes. Sci Signal 2021;14(710):eabj2807. https://doi.org/10.1126/scisignal.abj2807.

[74] Jaitin DA, Adlung L, Thaiss CA, Weiner A, Li B, Descamps H, et al. Lipid-associated macrophages control metabolic homeostasis in a trem2-dependent manner. Cell 2019;178(3). https://doi.org/10.1016/j.cell.2019.05.054.

[75] Jakobsson T, Venteclef N, Toresson G, Damdimopoulos AE, Ehrlund A, Lou X, et al. GPS2 is required for cholesterol efflux by triggering histone demethylation, LXR recruitment, and coregulator assembly at the ABCG1 locus. Mol Cell 2009;34(4). https://doi.org/10.1016/j.molcel.2009.05.006.

[76] Jeffery E, Church CD, Holtrup B, Colman L, Rodeheffer MS. Rapid depot-specific activation of adipocyte precursor cells at the onset of obesity. Nat Cell Biol 2015;17(4):376–85. https://doi.org/10.1038/ncb3122.

[77] Joseph A, Chen H, Anagnostopoulos G, Montégut L, Lafarge A, Motiño O, et al. Effects of acyl-coenzyme A binding protein (ACBP)/diazepam-binding inhibitor (DBI) on body mass index. Cell Death Dis 2021;12(6):599. https://doi.org/10.1038/s41419-021-03864-9.

[78] Kahai S, Vary CPH, Gao Y, Seth A. Collagen, type V, alpha1 (COL5A1) is regulated by TGF-beta in osteoblasts. Matrix Biol 2004;23(7):445–55. https://doi.org/10.1016/j.matbio.2004.09.004.

[79] Kahn JH, Goddi A, Sharma A, Heiman J, Carmona A, Li Y, et al. SMRT regulates metabolic homeostasis and adipose tissue macrophage phenotypes in tandem. Endocrinology 2020;161(10). https://doi.org/10.1210/endocr/bqaa132.

[80] Kalluri R, LeBleu VS. The biology, function, and biomedical applications of exosomes. Science 2020;367(6478). https://doi.org/10.1126/science.aau6977.

[81] Keerthikumar S, Chisanga D, Ariyaratne D, al Saffar H, Anand S, Zhao K, et al. ExoCarta: a web-based compendium of exosomal cargo. J Mol Biol 2016;428(4):688–92. https://doi.org/10.1016/j.jmb.2015.09.019.

[82] Kita S, Maeda N, Shimomura I. Interorgan communication by exosomes, adipose tissue, and adiponectin in metabolic syndrome. J Clin Investig 2019;129(10):4041–9. https://doi.org/10.1172/JCI129193.

[83] Kong P, Gonzalez-Quesada C, Li N, Cavalera M, Lee D-W, Frangogiannis NG. Thrombospondin-1 regulates adiposity and metabolic dysfunction in diet-induced obesity enhancing adipose inflammation and stimulating adipocyte proliferation. Am J Physiol Endocrinol Metab 2013;305(3):E439–50. https://doi.org/10.1152/ajpendo.00006.2013.

[84] Kuleshov M v, Jones MR, Rouillard AD, Fernandez NF, Duan Q, Wang Z, et al. Enrichr: a comprehensive gene set enrichment analysis web server 2016 update. Nucleic Acids Res 2016;44(W1):W90–7. https://doi.org/10.1093/nar/gkw377.

[85] Kumar R, Mickael C, Kassa B, Gebreab L, Robinson JC, Koyanagi DE, et al. TGF-β activation by bone marrow-derived thrombospondin-1 causes Schistosoma- and hypoxia-induced pulmonary hypertension. Nat Commun 2017;8:15494. https://doi.org/10.1038/ncomms15494.

[86] Lazar I, Clement E, Dauvillier S, Milhas D, Ducoux-Petit M, LeGonidec S, et al. Adipocyte exosomes promote melanoma aggressiveness through fatty acid oxidation: a novel mechanism linking obesity and cancer. Cancer Res 2016;76(14):4051–7. https://doi.org/10.1158/0008-5472.CAN-16-0651.

[87] Lee M-J, Pickering RT, Shibad V, Wu Y, Karastergiou K, Jager M, et al. Impaired glucocorticoid suppression of TGFβ signaling in human omental adipose tissues limits adipogenesis and may promote fibrosis. Diabetes 2019;68(3):587–97. https://doi.org/10.2337/db18-0955.

[88] Lee M-J, Wu Y, Fried SK. Adipose tissue heterogeneity: implication of depot differences in adipose tissue for obesity complications. Mol Aspect Med 2013;34(1). https://doi.org/10.1016/j.mam.2012.10.001.

[89] Lee Y-H, Mottillo EP, Granneman JG. Adipose tissue plasticity from WAT to BAT and in between. Biochim Biophys Acta 2014;1842(3). https://doi.org/10.1016/j.bbadis.2013.05.011.

[90] Lee Y-H, Petkova AP, Mottillo EP, Granneman JG. In vivo identification of bipotential adipocyte progenitors recruited by β3-adrenoceptor activation and high-fat feeding. Cell Metabol 2012;15(4):480–91. https://doi.org/10.1016/j.cmet.2012.03.009.

[91] Lei G-S, Kline HL, Lee C-H, Wilkes DS, Zhang C. Regulation of collagen V expression and epithelial-mesenchymal transition by miR-185 and miR-186 during idiopathic pulmonary fibrosis. Am J Pathol 2016;186(9):2310–6. https://doi.org/10.1016/j.ajpath.2016.04.015.

[92] Lentucci C, Belkina AC, Cederquist CT, Chan M, Johnson HE, Prasad S, et al. Inhibition of Ubc13-mediated ubiquitination by GPS2 regulates multiple stages of B cell development. J Biol Chem 2017;292(7):2754–72. https://doi.org/10.1074/jbc.M116.755132.

[93] Li H, Wang X, Rukina D, Huang Q, Lin T, Sorrentino V, et al. An integrated systems genetics and omics toolkit to probe gene function. Cell Systems 2018a;6(1):90–102.e4. https://doi.org/10.1016/j.cels.2017.10.016.

[94] Li H, Wang X, Rukina D, Huang Q, Lin T, Sorrentino V, et al. An integrated systems genetics and omics toolkit to probe gene function. Cell Systems 2018b;6(1):90–102.e4. https://doi.org/10.1016/j.cels.2017.10.016.

[95] Li P, Fan W, Xu J, Lu M, Yamamoto H, Auwerx J, et al. Adipocyte NCoR knockout decreases PPARγ phosphorylation and enhances PPARγ activity and insulin sensitivity. Cell 2011;147(4):815–26. https://doi.org/10.1016/j.cell.2011.09.050.

[96] Li S-N, Wu J-F. TGF-β/SMAD signaling regulation of mesenchymal stem cells in adipocyte commitment. Stem Cell Res Ther 2020;11(1):41. https://doi.org/10.1186/s13287-020-1552-y.

[97] Li Y, Hao Y, Owyang C. Diazepam-binding inhibitor mediates feedback regulation of pancreatic secretion and postprandial release of cholecystokinin. J Clin Investig 2000;105(3):351–9. https://doi.org/10.1172/JCI7204.

[98] Li Y, Tong X, Rumala C, Clemons K, Wang S. Thrombospondin1 deficiency reduces obesity-associated inflammation and improves insulin sensitivity in a diet-induced obese mouse model. PLoS One 2011;6(10):e26656. https://doi.org/10.1371/journal.pone.0026656.

[99] Liu Y, Lu X, Li X, Du P, Qin G. High-fat diet triggers obesity-related early infiltration of macrophages into adipose tissue and transient reduction of

blood monocyte count. Mol Immunol 2020;117:139–46. https://doi.org/10.1016/j.molimm.2019.11.002.

[100] Longo M, Zatterale F, Naderi J, Parrillo L, Formisano P, Raciti GA, et al. Adipose tissue dysfunction as determinant of obesity-associated metabolic complications. Int J Mol Sci 2019;20(9). https://doi.org/10.3390/ijms20092358.

[101] Lumeng CN, Liu J, Geletka L, Delaney C, Delproposto J, Desai A, et al. Aging is associated with an increase in T cells and inflammatory macrophages in visceral adipose tissue. J Immunol (Baltimore, MD: 1950) 2011;187(12):6208–16. https://doi.org/10.4049/jimmunol.1102188.

[102] Ma X, Lee P, Chisholm DJ, James DE. Control of adipocyte differentiation in different fat depots; implications for pathophysiology or therapy. Front Endocrinol 2015;6. https://doi.org/10.3389/fendo.2015.00001.

[103] Macdougall CE, Longhi MP. Adipose tissue dendritic cells in steady-state. Immunology 2019;156(3):228–34. https://doi.org/10.1111/imm.13034.

[104] Macdougall CE, Wood EG, Loschko J, Scagliotti V, Cassidy FC, Robinson ME, et al. Visceral adipose tissue immune homeostasis is regulated by the crosstalk between adipocytes and dendritic cell subsets. Cell Metabol 2018;27(3):588–601.e4. https://doi.org/10.1016/j.cmet.2018.02.007.

[105] Macotela Y, Emanuelli B, Mori MA, Gesta S, Schulz TJ, Tseng Y-H, et al. Intrinsic differences in adipocyte precursor cells from different white fat depots. Diabetes 2012;61(7):1691–9. https://doi.org/10.2337/db11-1753.

[106] Marcelin G, Ferreira A, Liu Y, Atlan M, Aron-Wisnewsky J, Pelloux V, et al. A PDGFRα-mediated switch toward CD9 high adipocyte progenitors controls obesity-induced adipose tissue fibrosis. Cell Metabol 2017;25(3):673–85. https://doi.org/10.1016/j.cmet.2017.01.010.

[107] Mathivanan S, Fahner CJ, Reid GE, Simpson RJ. ExoCarta 2012: database of exosomal proteins, RNA and lipids. Nucleic Acids Res 2012;40(D1):D1241–4. https://doi.org/10.1093/nar/gkr828.

[108] Mathivanan S, Ji H, Simpson RJ. Exosomes: extracellular organelles important in intercellular communication. J Proteonomics 2010;73(10):1907–20. https://doi.org/10.1016/j.jprot.2010.06.006.

[109] Mathivanan S, Simpson RJ. ExoCarta: a compendium of exosomal proteins and RNA. Proteomics 2009;9(21):4997–5000. https://doi.org/10.1002/pmic.200900351.

[110] Matsuo Y, Tanaka M, Yamakage H, Sasaki Y, Muranaka K, Hata H, et al. Thrombospondin 1 as a novel biological marker of obesity and metabolic syndrome. Metab, Clin Exp 2015;64(11):1490–9. https://doi.org/10.1016/j.metabol.2015.07.016.

[111] Merrick D, Sakers A, Irgebay Z, Okada C, Calvert C, Morley MP, et al. Identification of a mesenchymal progenitor cell hierarchy in adipose tissue. Science (New York, NY) 2019;(6438):364. https://doi.org/10.1126/science.aav2501.

[112] Minchin JEN, Dahlman I, Harvey CJ, Mejhert N, Singh MK, Epstein JA, et al. Plexin D1 determines body fat distribution by regulating the type V collagen microenvironment in visceral adipose tissue. Proc Natl Acad Sci USA 2015;112(14):4363–8. https://doi.org/10.1073/pnas.1416412112.

[113] Morris DL, Oatmen KE, Mergian TA, Cho KW, DelProposto JL, Singer K, et al. CD40 promotes MHC class II expression on adipose tissue macrophages and regulates adipose tissue CD4+ T cells with obesity. J Leukoc Biol 2016;99(6):1107–19. https://doi.org/10.1189/jlb.3A0115-009R.

[114] Morris DL, Singer K, Lumeng CN. Adipose tissue macrophages: phenotypic plasticity and diversity in lean and obese states. Curr Opin Clin Nutr Metab Care 2011;14(4):341–6. https://doi.org/10.1097/MCO.0b013e328347970b.

[115] Nahmgoong H, Jeon YG, Park ES, Choi YH, Han SM, Park J, et al. Distinct properties of adipose stem cell subpopulations determine fat depot-specific characteristics. Cell Metabol 2022. https://doi.org/10.1016/j.cmet.2021.11.014.

[116] Nakamura S, Takamura T, Matsuzawa-Nagata N, Takayama H, Misu H, Noda H, et al. Palmitate induces insulin resistance in H4IIEC3 hepatocytes through reactive oxygen species produced by mitochondria. J Biol Chem 2009;284(22):14809–18. https://doi.org/10.1074/jbc.M901488200.

[117] Nawaz A, Aminuddin A, Kado T, Takikawa A, Yamamoto S, Tsuneyama K, et al. CD206+ M2-like macrophages regulate systemic glucose metabolism by inhibiting proliferation of adipocyte progenitors. Nat Commun 2017;8(1):286. https://doi.org/10.1038/s41467-017-00231-1.

[118] Nawaz A, Tobe K. M2-like macrophages serve as a niche for adipocyte progenitors in adipose tissue. J Diabetes Invest 2019;10(6):1394–400. https://doi.org/10.1111/jdi.13114.

[119] Nofsinger RR, Li P, Hong S-H, Jonker JW, Barish GD, Ying H, et al. SMRT repression of nuclear receptors controls the adipogenic set point and metabolic homeostasis. Proc Natl Acad Sci USA 2008;105(50):20021–6. https://doi.org/10.1073/pnas.0811012105.

[120] Oberoi J, Fairall L, Watson PJ, Yang J-C, Czimmerer Z, Kampmann T, et al. Structural basis for the assembly of the SMRT/NCoR core transcriptional repression machinery. Nat Struct Mol Biol 2011;18(2):177–84. https://doi.org/10.1038/nsmb.1983.

[121] Orr JS, Kennedy AJ, Hasty AH. Isolation of adipose tissue immune cells. JoVE 2013;75:e50707. https://doi.org/10.3791/50707.

[122] Pegtel DM, Gould SJ. Exosomes. Annu Rev Biochem 2019;88:487–514. https://doi.org/10.1146/annurev-biochem-013118-111902.

[123] Petrus P, Mejhert N, Corrales P, Lecoutre S, Li Q, Maldonado E, et al. Transforming growth factor-β3 regulates adipocyte number in subcutaneous white adipose tissue. Cell Rep 2018a;25(3):551–560.e5. https://doi.org/10.1016/j.celrep.2018.09.069.

[124] Petrus P, Mejhert N, Corrales P, Lecoutre S, Li Q, Maldonado E, et al. Transforming growth factor-β3 regulates adipocyte number in subcutaneous white adipose tissue. Cell Rep 2018b;25(3):551–560.e5. https://doi.org/10.1016/j.celrep.2018.09.069.

[125] Prunet-Marcassus B, Cousin B, Caton D, André M, Pénicaud L, Casteilla L. From heterogeneity to plasticity in adipose tissues: site-specific differences. Exp Cell Res 2006;312(6). https://doi.org/10.1016/j.yexcr.2005.11.021.

[126] Qu Y, Zhang Q, Cai X, Li F, Ma Z, Xu M, et al. Exosomes derived from miR-181-5p-modified adipose-derived mesenchymal stem cells prevent liver fibrosis via autophagy activation. J Cell Mol Med 2017;21(10):2491–502. https://doi.org/10.1111/jcmm.13170.

[127] Rahimi N, Tremblay E, McAdam L, Roberts A, Elliott B. Autocrine secretion of TGF-beta 1 and TGF-beta 2 by pre-adipocytes and adipocytes: a potent negative regulator of adipocyte differentiation and proliferation of mammary carcinoma cells. In Vitro Cell Dev Biol Anim 1998;34(5):412–20. https://doi.org/10.1007/s11626-998-0023-z.

[128] Rajbhandari P, Arneson D, Hart SK, Ahn IS, Diamante G, Santos LC, et al. Single cell analysis reveals immune cell-adipocyte crosstalk regulating the transcription of thermogenic adipocytes. Elife 2019;8. https://doi.org/10.7554/eLife.49501.

[129] Remsberg JR, Ediger BN, Ho WY, Damle M, Li Z, Teng C, et al. Deletion of histone deacetylase 3 in adult beta cells improves glucose tolerance via increased insulin secretion. Mol Metabol 2017;6(1):30–7. https://doi.org/10.1016/j.molmet.2016.11.007.

[130] Rodeheffer MS, Birsoy K, Friedman JM. Identification of white adipocyte progenitor cells in vivo. Cell 2008;135(2):240–9. https://doi.org/10.1016/j.cell.2008.09.036.

[131] Rohm M, Sommerfeld A, Strzoda D, Jones A, Sijmonsma TP, Rudofsky G, et al. Transcriptional cofactor TBLR1 controls lipid mobilization in white adipose tissue. Cell Metabol 2013;17(4):575–85. https://doi.org/10.1016/j.cmet.2013.02.010.

[132] Rondini EA, Granneman JG. Single cell approaches to address adipose tissue stromal cell heterogeneity. Biochem J 2020;477(3). https://doi.org/10.1042/BCJ20190467.

[133] Rosen ED, Spiegelman BM. Adipocytes as regulators of energy balance and glucose homeostasis. Nature 2006;444(7121). https://doi.org/10.1038/nature05483.

[134] Russo L, Lumeng CN. Properties and functions of adipose tissue macrophages in obesity. Immunology 2018;155(4):407–17. https://doi.org/10.1111/imm.13002.

[135] Samad F, Yamamoto K, Pandey M, Loskutoff DJ. Elevated expression of transforming growth factor-beta in adipose tissue from obese mice. Mol Med (Cambridge, MA) 1997;3(1):37–48.

[136] Sanyal S, Båvner A, Haroniti A, Nilsson L-M, Lundåsen T, Rehnmark S, et al. Involvement of corepressor complex subunit GPS2 in transcriptional pathways governing human bile acid biosynthesis. Proc Natl Acad Sci USA 2007;104(40):15665–70. https://doi.org/10.1073/pnas.0706736104.

[137] Sárvári AK, van Hauwaert EL, Markussen LK, Gammelmark E, Marcher A-B, Ebbesen MF, et al. Plasticity of epididymal adipose tissue in response to diet-induced obesity at single-nucleus resolution. Cell Metabol 2021;33(2):437–453.e5. https://doi.org/10.1016/j.cmet.2020.12.004.

[138] Schadt EE, Molony C, Chudin E, Hao K, Yang X, Lum PY, et al. Mapping the genetic architecture of gene expression in human liver. PLoS Biol 2008;6(5):e107. https://doi.org/10.1371/journal.pbio.0060107.

[139] Schwalie PC, Dong H, Zachara M, Russeil J, Alpern D, Akchiche N, et al. A stromal cell population that inhibits adipogenesis in mammalian fat depots. Nature 2018;559(7712):103–8. https://doi.org/10.1038/s41586-018-0226-8.

[140] Sherman BT, Hao M, Qiu J, Jiao X, Baseler MW, Lane HC, et al. DAVID: a web server for functional enrichment analysis and functional annotation of gene lists (2021 update). Nucleic Acids Res 2022. https://doi.org/10.1093/nar/gkac194.

[141] Shimizu H, Lu Y, Vella KR, Damilano F, Astapova I, Amano I, et al. Nuclear corepressor SMRT is a strong regulator of body weight independently of its ability to regulate thyroid hormone action. PLoS One 2019;14(8):e0220717. https://doi.org/10.1371/journal.pone.0220717.

[142] Sica V, Martins I, Motiño O, Bravo-San Pedro JM, Kroemer G. Antibody-mediated neutralization of ACBP/DBI has anorexigenic and lipolytic effects. Adipocyte 2020;9(1):116–9. https://doi.org/10.1080/21623945.2020.1736734.

[143] Simpson RJ, Kalra H, Mathivanan S. ExoCarta as a resource for exosomal research. J Extracell Vesicles 2012;1. https://doi.org/10.3402/jev.v1i0.18374.

[144] Smith U, Kahn BB. Adipose tissue regulates insulin sensitivity: role of adipogenesis, de novo lipogenesis and novel lipids. J Intern Med 2016;280(5). https://doi.org/10.1111/joim.12540.

[145] Soedono S, Cho KW. Adipose tissue dendritic cells: critical regulators of obesity-induced inflammation and insulin resistance. Int J Mol Sci 2021;22(16). https://doi.org/10.3390/ijms22168666.

[146] Spain BH, Bowdish KS, Pacal AR, Staub SF, Koo D, Chang CY, et al. Two human cDNAs, including a homolog of Arabidopsis FUS6 (COP11), suppress G-protein- and mitogen-activated protein kinase-mediated signal transduction in yeast and mammalian cells. Mol Cell Biol 1996;16(12). https://doi.org/10.1128/MCB.16.12.6698.

[147] Stefanovic-Racic M, Yang X, Turner MS, Mantell BS, Stolz DB, Sumpter TL, et al. Dendritic cells promote macrophage infiltration and comprise a substantial proportion of obesity-associated increases in CD11c+ cells in adipose tissue and liver. Diabetes 2012;61(9):2330–9. https://doi.org/10.2337/db11-1523.

[148] Stenina-Adognravi O. Invoking the power of thrombospondins: regulation of thrombospondins expression. Matrix Biol 2014;37:69–82. https://doi.org/10.1016/j.matbio.2014.02.001.

[149] Stephens JM. The fat controller: adipocyte development. PLoS Biol 2012;10(11). https://doi.org/10.1371/journal.pbio.1001436.

[150] Sun K, Kusminski CM, Scherer PE. Adipose tissue remodeling and obesity. J Clin Investig 2011;121(6). https://doi.org/10.1172/JCI45887.

[151] Tchkonia T, Giorgadze N, Pirtskhalava T, Tchoukalova Y, Karagiannides I, Forse RA, et al. Fat depot origin affects adipogenesis in primary cultured and cloned human preadipocytes. Am J Physiol Regul Integr Comp Physiol 2002;282(5):R1286–96. https://doi.org/10.1152/ajpregu.00653.2001.

[152] Tkach M, Théry C. Communication by extracellular vesicles: where we are and where we need to go. Cell 2016;164(6):1226–32. https://doi.org/10.1016/j.cell.2016.01.043.

[153] Toubal A, Clément K, Fan R, Ancel P, Pelloux V, Rouault C, et al. SMRT-GPS2 corepressor pathway dysregulation coincides with obesity-linked adipocyte inflammation. J Clin Investig 2013;123(1). https://doi.org/10.1172/JCI64052.

[154] Toyoda S, Shin J, Fukuhara A, Otsuki M, Shimomura I. Transforming growth factor β1 signaling links extracellular matrix remodeling to intracellular lipogenesis upon physiological feeding events. J Biol Chem 2022;298(4):101748. https://doi.org/10.1016/j.jbc.2022.101748.

[155] Traag VA, Waltman L, van Eck NJ. From Louvain to Leiden: guaranteeing well-connected communities. Sci Rep 2019;9(1):5233. https://doi.org/10.1038/s41598-019-41695-z.

[156] Varma V, Yao-Borengasser A, Bodles AM, Rasouli N, Phanavanh B, Nolen GT, et al. Thrombospondin-1 is an adipokine associated with obesity, adipose inflammation, and insulin resistance. Diabetes 2008;57(2):432–9. https://doi.org/10.2337/db07-0840.

[157] Venteclef N, Jakobsson T, Ehrlund A, Damdimopoulos A, Mikkonen L, Ellis E, et al. GPS2-dependent corepressor/SUMO pathways govern anti-inflammatory actions of LRH-1 and LXRbeta in the hepatic acute phase response. Genes Dev 2010;24(4). https://doi.org/10.1101/gad.545110.

[158] Vijay J, Gauthier M-F, Biswell RL, Louiselle DA, Johnston JJ, Cheung WA, et al. Single-cell analysis of human adipose tissue identifies depot and disease specific cell types. Nat Metabol 2020;2(1). https://doi.org/10.1038/s42255-019-0152-6.

[159] Vishvanath L, Gupta RK. Contribution of adipogenesis to healthy adipose tissue expansion in obesity. J Clin Invest 2019;129(10):4022–31. https://doi.org/10.1172/JCI129191.

[160] Wang QA, Tao C, Gupta RK, Scherer PE. Tracking adipogenesis during white adipose tissue development, expansion and regeneration. Nat Med 2013;19(10). https://doi.org/10.1038/nm.3324.

[161] Weinstock A, Brown EJ, Garabedian ML, Pena S, Sharma M, Lafaille J, et al. Single-cell RNA sequencing of visceral adipose tissue leukocytes reveals that caloric restriction following obesity promotes the accumulation of a distinct macrophage population with features of phagocytic cells. Immunometabolism 2019;1. https://doi.org/10.20900/immunometab20190008.

[162] Wen J, Ma Z, Livingston MJ, Zhang W, Yuan Y, Guo C, et al. Decreased secretion and profibrotic activity of tubular exosomes in diabetic kidney disease. Am J Physiol Ren Physiol 2020;319(4):F664–73. https://doi.org/10.1152/ajprenal.00292.2020.

[163] Westcott GP, Emont MP, Li J, Jacobs C, Tsai L, Rosen ED. Mesothelial cells are not a source of adipocytes in mice. Cell Rep 2021;36(2):109388. https://doi.org/10.1016/j.celrep.2021.109388.

[164] Wolf FA, Angerer P, Theis FJ. SCANPY: large-scale single-cell gene expression data analysis. Genome Biol 2018;19(1):15. https://doi.org/10.1186/s13059-017-1382-0.

[165] Xie Z, Bailey A, Kuleshov Mv, Clarke DJB, Evangelista JE, Jenkins SL, et al. Gene set knowledge discovery with Enrichr. Curr Protoc 2021;1(3). https://doi.org/10.1002/cpz1.90.

[166] Xie Z, Wang X, Liu X, Du H, Sun C, Shao X, et al. Adipose-derived exosomes Exert proatherogenic effects by regulating macrophage foam cell formation and polarization. J Am Heart Assoc 2018;7(5). https://doi.org/10.1161/JAHA.117.007442.

[167] Yadav H, Quijano C, Kamaraju AK, Gavrilova O, Malek R, Chen W, et al. Protection from obesity and diabetes by blockade of TGF-β/smad3 signaling. Cell Metabol 2011;14(1):67–79. https://doi.org/10.1016/j.cmet.2011.04.013.

[168] Yang E, Wang X, Gong Z, Yu M, Wu H, Zhang D. Exosome-mediated metabolic reprogramming: the emerging role in tumor microenvironment remodeling and its influence on cancer progression. Signal Transduct Targeted Ther 2020;5(1):242. https://doi.org/10.1038/s41392-020-00359-5.

[169] Yu Y, Du H, Wei S, Feng L, Li J, Yao F, et al. Adipocyte-derived exosomal MiR-27a induces insulin resistance in skeletal muscle through repression of PPARγ. Theranostics 2018;8(8):2171–88. https://doi.org/10.7150/thno.22565.

[170] Yuzefovych L v, Musiyenko SI, Wilson GL, Rachek LI. Mitochondrial DNA damage and dysfunction, and oxidative stress are associated with endoplasmic reticulum stress, protein degradation and apoptosis in high fat diet-induced insulin resistance mice. PLoS One 2013;8(1):e54059. https://doi.org/10.1371/journal.pone.0054059.

[171] Żbikowski A, Błachnio-Zabielska A, Galli M, Zabielski P. Adipose-derived exosomes as possible players in the development of insulin resistance. Int J Mol Sci 2021;22(14). https://doi.org/10.3390/ijms22147427.

[172] Zhang B, Yang Y, Xiang L, Zhao Z, Ye R. Adipose-derived exosomes: a novel adipokine in obesity-associated diabetes. J Cell Physiol 2019;234(10):16692–702. https://doi.org/10.1002/jcp.28354.

[173] Zhang DX, Vu LT, Ismail NN, Le MTN, Grimson A. Landscape of extracellular vesicles in the tumour microenvironment: interactions with stromal cells and with non-cell components, and impacts on metabolic reprogramming, horizontal transfer of neoplastic traits, and the emergence of therapeutic resistance. Semin Cancer Biol 2021;74:24–44. https://doi.org/10.1016/j.semcancer.2021.01.007.

[174] Zhang J, Kalkum M, Chait BT, Roeder RG. The N-CoR-HDAC3 nuclear receptor corepressor complex inhibits the JNK pathway through the integral subunit GPS2. Mol Cell 2002;9(3):611–23. https://doi.org/10.1016/s1097-2765(02)00468-9.

[175] Zhang L, Li Z, Skrzypczynska KM, Fang Q, Zhang W, O'Brien SA, et al. Single-cell analyses inform mechanisms of myeloid-targeted therapies in colon cancer. Cell 2020;181(2):442–459.e29. https://doi.org/10.1016/j.cell.2020.03.048.

[176] Zhang S, Wang L, Li S, Zhang W, Ma X, Cheng G, et al. Identification of potential key genes associated with adipogenesis through integrated analysis of five mouse transcriptome datasets. Int J Mol Sci 2018;19(11). https://doi.org/10.3390/ijms19113557.

[177] Zhao H, Shang Q, Pan Z, Bai Y, Li Z, Zhang H, et al. Exosomes from adipose-derived stem cells attenuate adipose inflammation and obesity through polarizing M2 macrophages and beiging in white adipose tissue. Diabetes 2018;67(2):235–47. https://doi.org/10.2337/db17-0356.

[178] Zheng C, Yang Q, Xu C, Shou P, Cao J, Jiang M, et al. CD11b regulates obesity-induced insulin resistance via limiting alternative activation and proliferation of adipose tissue macrophages. Proc Natl Acad Sci USA 2015;112(52):E7239–48. https://doi.org/10.1073/pnas.1500396113.

[179] Zheng GXY, Terry JM, Belgrader P, Ryvkin P, Bent ZW, Wilson R, et al. Massively parallel digital transcriptional profiling of single cells. Nat Commun 2017;8:14049. https://doi.org/10.1038/ncomms14049.

[180] Zhou X, Li Z, Qi M, Zhao P, Duan Y, Yang G, et al. Brown adipose tissue-derived exosomes mitigate the metabolic syndrome in high fat diet mice. Theranostics 2020;10(18):8197–210. https://doi.org/10.7150/thno.43968.

